Project Report
NOAA-35

Monetized Weather Radar Network Benefits for Tornado Cost Reduction

J. Y. N. Cho
J. M. Kurdzo

29 August 2019

Lincoln Laboratory
MASSACHUSETTS INSTITUTE OF TECHNOLOGY
LEXINGTON, MASSACHUSETTS

Prepared for the National Oceanic and Atmospheric Administration

This report is the result of studies performed at Lincoln Laboratory, a federally funded research and development center operated by Massachusetts Institute of Technology. This material is based on work supported by the National Oceanic and Atmospheric Administration under Air Force Contract No. FA8702-15-D-0001. Any opinions, findings, conclusions, or recommendations expressed in this material are those of the authors and do not necessarily reflect the views of the National Oceanic and Atmospheric Administration.

Massachusetts Institute of Technology
Lincoln Laboratory

Monetized Weather Radar Network Benefits for Tornado Cost Reduction

J.Y.N. Cho
J. M. Kurdzo
Group 43

Project Report NOAA-35

29 August 2019

Lexington Massachusetts

This page intentionally left blank.

EXECUTIVE SUMMARY

A monetized tornado benefit model is developed for arbitrary weather radar network configurations. Geospatial regression analyses indicate that improvement in two key radar coverage parameters—fraction of vertical space observed and cross-range horizontal resolution—lead to better tornado warning performance as characterized by tornado detection probability and false alarm ratio. Previous experimental results showing faster volume scan rates yielding greater warning performance, including increased lead times, are also incorporated into the model. Enhanced tornado warning performance, in turn, reduces casualty rates. In combination, then, it is clearly established that better and faster radar observations reduce tornado casualty rates. Furthermore, lower false alarm ratios save cost by cutting down on people's time lost while taking shelter.

The model is run on the existing contiguous United States weather radar network as well as hypothetical configurations. Key results are as follows (values are given in 2019 dollars):

1. Current weather radars provide a tornado-based benefit of $535M per year.

2. The remaining benefit pool is $676M per year.

3. About half of the benefit pool ($333M per year) can be claimed by upgrading the current radars with rapid-scan (one-minute volume coverage update) capability.

4. Over 99% of the current tornado-related benefit is realized east of the Rockies.

5. The highest single-site gap-filling benefit exists in northern Alabama and is about $4M per year ($7M per year with rapid scan capability).

The model also enabled estimation of the present-day net benefit (casualty reduction benefit minus sheltering cost) of tornado warnings ($1921M per year), as well as the benefit associated with the transition from county-based to storm-based tornado warnings ($732M per year).

The quantification of rapid scan effects is based on a small number of past experiments and is less robust than the other parts of the benefit model. In order to drive down this uncertainty, it is recommended that more statistics be gathered on the effects of faster volume scans on tornado warning performance by utilizing existing and new radars capable of fine temporal resolution observations.

This page intentionally left blank.

TABLE OF CONTENTS

This page intentionally left blank.

LIST OF ILLUSTRATIONS

LIST OF ILLUSTRATIONS
(Continued)

LIST OF TABLES

LIST OF TABLES
(Continued)

1. INTRODUCTION

For decades, the Weather Surveillance Radar-1988 Doppler (WSR-88D) network (Crum and Alberty 1993) has served as the backbone for severe weather observation in the U.S. Deployment of the WSR-88D led to significant improvement in severe weather warning performance (Polger et al. 1994). Upgrades to various subsystems over the years have kept its performance close to the leading edge of meteorological radar technology. In particular, the addition of dual polarization capability (Istok et al. 2009b) has provided major additional benefits for WSR-88D users.

There is, however, a limit to further upgrades. For example, meteorologists always want faster observational updates. Although some inroads have been made in this direction through the adoption of adaptive volume scan strategies (Chrisman 2013; Chrisman 2014), the mechanically steered antenna ultimately limits the ability of the WSR-88D to collect data quickly and adaptively in real time. A potential solution to this issue is the electronically scanned phased array radar (PAR). Although long considered too expensive for civilian applications, recent breakthroughs in cost reduction is bringing this technology within reach of a wider customer base (Herd and Conway 2016).

For over a decade, the National Oceanic and Atmospheric Administration (NOAA) has been studying PAR use for weather (Forsyth et al. 2005), with an eye toward possibly replacing the WSR-88D with a polarimetric PAR (PPAR) in the future. Although there are many potential benefits to deploying a PPAR nationally, there are also still many technical challenges to overcome (Zhang 2008). A solid business case will have to be built before such a large acquisition decision can be made. In response to this programmatic need, NOAA is conducting PPAR risk reduction and benefit quantification studies (Weber et al. 2018). The work described in this report is part of this effort; it covers benefit analyses for future weather radar networks with respect to tornadoes. A separate article covers a similar study for flash floods (Cho and Kurdzo 2019b).

NOAA is also an interested party in the ongoing Spectrum Efficient National Surveillance Radar (SENSR) program, which was initiated in 2016 to study the feasibility of auctioning at least 30 MHz of the federally reserved 1300–1350 MHz band by 2024 for commercial use (FAA 2018). SENSR is a multi-agency coalition composed of the Federal Aviation Administration (FAA), Department of Defense (DoD), and Department of Homeland Security (DHS); it is led by the FAA. Auction proceeds would fund the replacement surveillance capability of the long-range radars (LRRs) now operating in the 1300–1350-MHz band. Since 2700–2900 MHz is a potential target band for the LRR replacement sensors, the WSR-88D network could be impacted by the outcome of SENSR. It is also possible that some of the new radars deployed by SENSR could have weather observation capabilities that may be of utility for NOAA. Therefore, potential SENSR radar network solutions are considered as part of this study.

This page intentionally left blank.

2. BENEFIT MODEL

Excessive heat, tornadoes, and floods are the top three weather causes of fatalities in the U.S. (NOAA 2018). Tornado warnings issued by the National Weather Service (NWS) are part of a strategy to reduce casualties by providing people with a chance to shelter in advance (Simmons and Sutter 2011). Forecasters issuing these warnings utilize multiple data sources, with Doppler weather radar serving as the most essential component (Brotzge and Donner 2013). Indeed, the nation-wide deployment of the WSR-88D improved tornado warning statistics (Bieringer and Ray 1996) that led to an estimated casualty rate reduction of ~40% (Simmons and Sutter 2005).

Decreasing tornado casualties is just one of many weather radar benefits to society. These radars, however, are expensive to operate and maintain, and even more so to replace. As the WSR-88Ds approach the end of their original (and upgraded) life spans (NRC 2002), careful consideration must be given to defining requirements for their replacements or further refurbishments to optimize return on investment. Spatial coverage, measurement resolution, update rates, and sensitivity are all important performance metrics that should be maximized, but there is a cost associated with each. Benefit quantification based on radar performance and network layout can help with difficult decisions and enable objective trade-offs.

This chapter presents a geospatial model for monetizing tornado-related benefits of a generic weather radar network. The goal of this effort was to take as input an arbitrary network of weather radars over a given area, and output a monetized benefit that the radars provide to the area populace with respect to tornadoes. Given that this is a complex problem involving many factors, we endeavored to simplify the model components to only the essentials needed to objectively quantify the radar effects. Statistically insignificant variables were not used. In cases of uncertainty, we took a conservative approach. As the overwhelming majority of tornadoes in the nation are within the contiguous United States (CONUS), we took that to be our geographic scope. The model can easily be expanded to include the rest of the U.S., but the increase in benefit should be marginal, since we calculated that only 0.09% of U.S. tornadoes occur outside the CONUS historically.

Tornadoes are relatively rare occurrences, and casualties (especially fatalities) are sparser. To achieve statistically significant results, we had to use as much data as we could, which meant including as many years of historical data as possible. However, this imperative was counteracted by the need to maintain a uniform condition set for fair regression results. This issue will be addressed in the individual analysis subsections.

2.1 RADAR DATA SOURCE FOR MODEL DEVELOPMENT

In the CONUS, there are 143 operational WSR-88Ds. There are also 44 FAA Terminal Doppler Weather Radars (TDWRs) (Michelson et al. 1990) in the CONUS. The TDWRs' primary mission is providing hazardous wind-shear alerts for aircraft landing and taking off at airports, but their data are also

available to forecasters and the public (Istok et al. 2009a). Compared to the WSR-88D, they provide faster low-level updates (every minute during hazardous weather conditions) and better vertical resolution. However, the TDWR's operation is more negatively impacted by rain attenuation and range-velocity ambiguity issues (Cho and Weber 2010) due to the utilization of C band rather than S band that the WSR-88D uses.

In areas with TDWR coverage, do meteorologists make use of this additional radar data for making tornado warning decisions? To answer this question, we conducted a small survey that targeted NWS offices with TDWR coverage, including both tornado-intensive and tornado-sparse locations. We received responses from eight forecast offices (Tampa Bay, Florida; Peachtree City, Georgia; Wilmington, Ohio; Norman, Oklahoma; Fort Worth, Texas; Philadelphia, Pennsylvania; Topeka, Kansas; and Milwaukee, Wisconsin), plus the Storm Prediction Center (SPC). The survey prompt, as posed, is included below, and is followed by the responses from the forecasters. Some of the responses were lightly edited for brevity and focus.

Prompt

NOAA has tasked Lincoln Laboratory with assessing future radar network designs with respect to tornado warning lead time. Rather than focusing on temporal update rate, which has been a common area of research, we will be focusing on spatial resolution and height of the beam (resulting from different network configurations). We are at the stage of deciding whether or not to include TDWRs in our analysis on tornado warning lead time. If you could give a brief response on whether or not you find that TDWR is regularly used for tornado warning guidance in your office, we would appreciate your thoughts.

Responses

Tampa Bay Area, FL: "We do have a TDWR located at the north end of Tampa Bay. It is used regularly when storms are near the bay, especially for waterspout detection and strong marine downbursts. Of course, TDWR comes with several caveats. Data is often messy and/or incomplete and NWS offices don't really control if or when they are taken down for maintenance. Just a few considerations."

Peachtree City, GA: "Regarding the TDWR (for us at FFC [Weather Forecast Office in Peachtree City, Georgia] we use TATL [Terminal Doppler Weather Radar in Atlanta, Georgia])... I would say for us in ATL [Atlanta] we routinely use it during warning operations, especially around the ATL metro. In fact, it was the only source we had during the missed tornado/tornado warning at Hartsfield-Jackson Airport this past spring. It captured a very small velocity couplet right over the airport when looking back at the data, whereas KFFC [Weather Surveillance Radar-1988 Doppler in Peachtree City, Georgia] (which is not too far) had nothing. While I would still say that we use the 88Ds MUCH more when issuing tornado warnings, our TDWR is very useful in many cases, particularly squall lines in our area. I'd say include TDWRs in your analysis if you can!"

Wilmington, OH: “Here at ILN [Weather Forecast Office in Wilmington, Ohio], we are very fortunate to have 3 TDWRs (TDAY, TCVG, TCMH [Terminal Doppler Weather Radars in Dayton, Ohio; Covington, Kentucky; and Columbus, Ohio]) in our CWA [county warning area]. And yes, we heavily rely on them for issuance of TORs [tornado warnings]. I would say we issue more TORs based on TDWRs signals than we do from our 88-D (KILN [Weather Surveillance Radar-1988 Doppler in Wilmington, Ohio]). Given that many of our tornadoes are spawned courtesy of QLCSs [quasi-linear convective systems] (and therefore have very quick spin-ups and lifespans), TDWR data is constantly used in the warning decision process for our office.”

Norman, OK: “We absolutely use TDWR to assist with tornado warning decisions. It’s been a great tool in numerous events close to metro OKC [Oklahoma City], especially when there is the potential for tornadic storms close to the radar. There is utility in sampling closer to the storm—especially for QLCS/non-supercell tornado events.”

SPC, Norman, OK: “While I don't issue warnings at SPC, I do get to see tornado warnings issued from every office across the CONUS. From what I’ve noticed, TDWRs do occasionally provide useful velocity data that wouldn't otherwise be seen by the WSR-88D network. Specifically, I’ve seen this multiple times along the FL Peninsula for mainly land-falling tropical systems, and in western NC with TCLT [Terminal Doppler Weather Radar in Charlotte, North Carolina] where there is a bit of a radar hole otherwise. Prior to the SAILS/MESO-SAILS [supplemental adaptive intra-volume low-level scan/multiple-elevation scan option for supplemental adaptive intra-volume low-level scan] era, TDWR velocity data had much higher temporal resolution than the 88Ds, so I believe offices would often use them to get better looks at velocity couplets in between 88D scans. I know OUN [Weather Forecast Office in Norman, Oklahoma] did this with TOKC [Terminal Doppler Weather Radar in Oklahoma City, Oklahoma] back when I volunteered with them years ago.”

Fort Worth, TX: “TDWR is something we make aggressive use of for warning decisions at the Fort Worth WFO [Weather Forecast Office]. The high temporal and spatial resolution of these systems is paramount in fast-evolving tornadic events like those spawned by QLCSs. I think this is where the TDWRs shine for us when it comes to tornado warning guidance; while we can usually ‘see’ and track the big ones well enough from KFWS [Weather Surveillance Radar-1988 Doppler in Fort Worth, Texas], it’s nice having the finer detail from way down low with the TDWRs when small and low-level mesocylones are a threat. Obviously, we have to make due with increased velocity dealiasing failures, attenuation, and beam blockage, but I’d still put the TDWRs up there on the ‘must-have’ list for tornado warning guidance.”

Philadelphia, PA: “I’ve used TPHL [Terminal Doppler Weather Radar in Philadelphia, Pennsylvania] more times than I count to either help verify what KDIX [Weather Surveillance Radar-1988 Doppler in Fort Dix, New Jersey] was showing rotation-wise or just straight up warning based solely off its signatures. TDWRs helped a lot too on MD’s eastern shore using either TBWI [Terminal Doppler Weather Radar in Baltimore, Maryland] or TADW [Terminal Doppler Weather Radar in Andrews Air Force Base, Maryland]. Same can be said for TEWR [Terminal Doppler Weather Radar in Newark, New Jersey]. Again these Terminal Dopplers have become an amazing asset to warning operations.”

Topeka, KS: “Here at Topeka, TMCI [Terminal Doppler Weather Radar in Kansas City, Missouri] does clip a few of our NE counties. I have not personally had the opportunity to use the TDWR for tornado warning guidance, but I imagine that on the rare occasions that we have tornadic storms within range of the radar that we would use it. I am all for increasing the spatial resolution of the current 88-D network by any means possible.”

Milwaukee/Sullivan, WI: “The Milwaukee TDWR is mainly a source of supplemental information during severe weather operations. The most common use would be to get a different perspective on storm structure if the 88D’s data is being contaminated by TBSS [three-body scatter signature], etc.”

The responses unanimously affirmed the TDWR as a useful data source for tornado warning decisions. Although the reliance ratio on data from WSR-88Ds and TDWRs varied depending on their relative coverages, note that one office (Wilmington) even asserted that they issued more tornado warnings based on TDWR data than on WSR-88D data. Consequently, we decided to include TDWRs as part of our analysis. Figure 2-1 is a map of CONUS WSR-88D and TDWR locations.

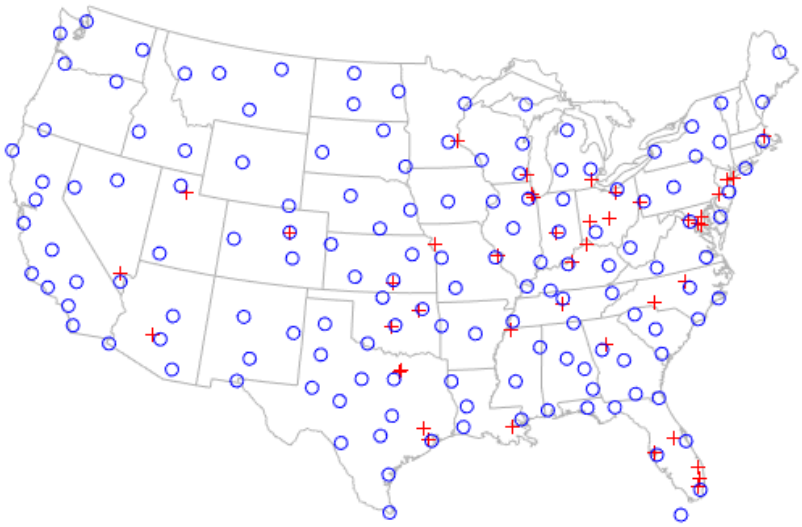

Figure 2-1. CONUS WSR-88D (blue circle) and TDWR (red cross) locations.

2.2 RADAR COVERAGE AND RESOLUTION METRICS

Past studies of tornado warning performance dependence on weather radar have used distance from radar as the key parameter (Brotzge and Erickson 2009; Brotzge et al. 2011; Brotzge et al. 2013). This

makes sense because sensitivity, spatial resolution, and low-level coverage degrade with range. Tornadoes exist within a limited height above the surface and their rotational signature requires fine horizontal resolution to detect. Our initial investigation into the relationship between radar coverage and tornado warning performance, however, exposed some unexpected behavior at close range. We hypothesized that this was due to not taking into account near-radar degraded coverage caused by the "cone of silence." Weather radars do not scan all the way to zenith angle, which leaves an overhead cone of unobserved space. Some of this gap can be covered if there is another radar close enough, but the spatial resolution is degraded. Even if a radar did scan to zenith, it would not be able to measure horizontal velocity as the angle would be too steep.

Why is radar coverage aloft important for tornado warning decisions even though tornadoes occur at the surface? The ultimate goal is to issue a warning before a tornado touches down with as much lead time as possible, and forecasters look for features at both low- and mid-levels. For supercell storms, these include a strong mesocyclone, a bounded weak echo region or a hook echo in conjunction with big peak mid-level reflectivities, and a mid-level overhang (Lemon and Doswell 1979; Falk 1997). Virtually all strong or violent tornadoes are associated with mesocyclones (Burgess and Lemon 1990). Detection of tornado debris signatures aloft after touchdown is also used for detection and confirmation, with violent tornadoes sending debris to over 18,000 ft above ground level (AGL) (Schultz et al. 2012; Gibbs 2016). The cone of silence cuts off these critical measurements.

Thus, we developed a new radar coverage metric, fraction of vertical volume observed (FVO), with the floor at the Earth's surface and ceiling at 20 kft AGL. The top panel of Figure 2-2 shows the vertical observation limits vs. range for a WSR-88D on a smooth Earth. The bottom plot shows FVO with range, illustrating that this metric combines the cone of silence and Earth curvature effects. In the actual calculation, we included surface elevation data to account for blockage and height AGL variations. We used Level 1 Shuttle Radar Tomography Mission (SRTM) data, which includes both natural terrain and surface structures/features, as the primary source of digital elevation, supplemented by Level 1 Digital Terrain Elevation Data (DTED) where SRTM had gaps (Cho 2015). Our model computation grid matched the horizontal resolution (30 arcsec in latitude and longitude) of these data sets, while the vertical grid spacing was 200 ft. We employed a standard 4/3-Earth-radius model for radio frequency (RF) propagation path calculations. The minimum elevation coverage angle was taken to be 0° (roughly corresponding to the bottom side of the main lobe) for both WSR-88D and TDWR, while the maximum angle was set to 20° for WSR-88D and 60° for TDWR (topside of the main lobe). These are approximations, since the minimum and maximum angles vary from site to site (especially for TDWRs) and for different scan strategies (especially for WSR-88Ds).

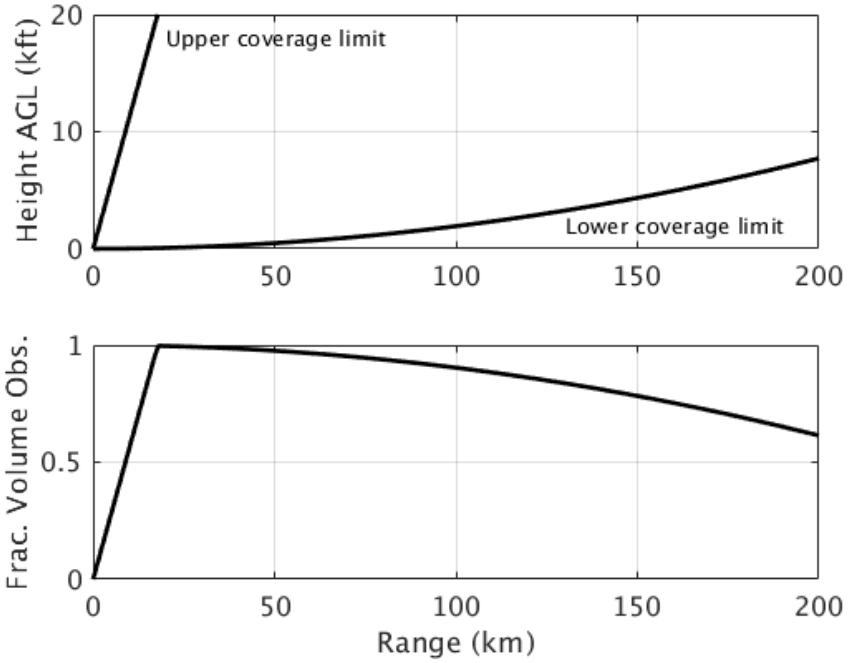

Figure 2-2. (Top) WSR-88D vertical coverage limits vs. range from radar as delineated by the bottom of the lowest-elevation scan (0°) and the top of the highest-elevation scan (20°). The 4/3-Earth-radius propagation model is used. (Bottom) Corresponding fraction of vertical volume observed between 0 and 20 kft AGL.

The 20-kft value for the FVO ceiling was chosen because above this height the CONUS coverage by the WSR-88D network is essentially perfect (Figure 2-3). Since we are developing statistical relationships based on historical data (i.e., on observations by existing radars), increasing the ceiling of this coverage metric does not add any informational value. In other words, the surface-to-20-kft AGL span covers the entire dynamic range of fractional vertical volume observed. Figure 2-4 shows the resulting FVO over the CONUS for the combined WSR-88D and TDWR networks.

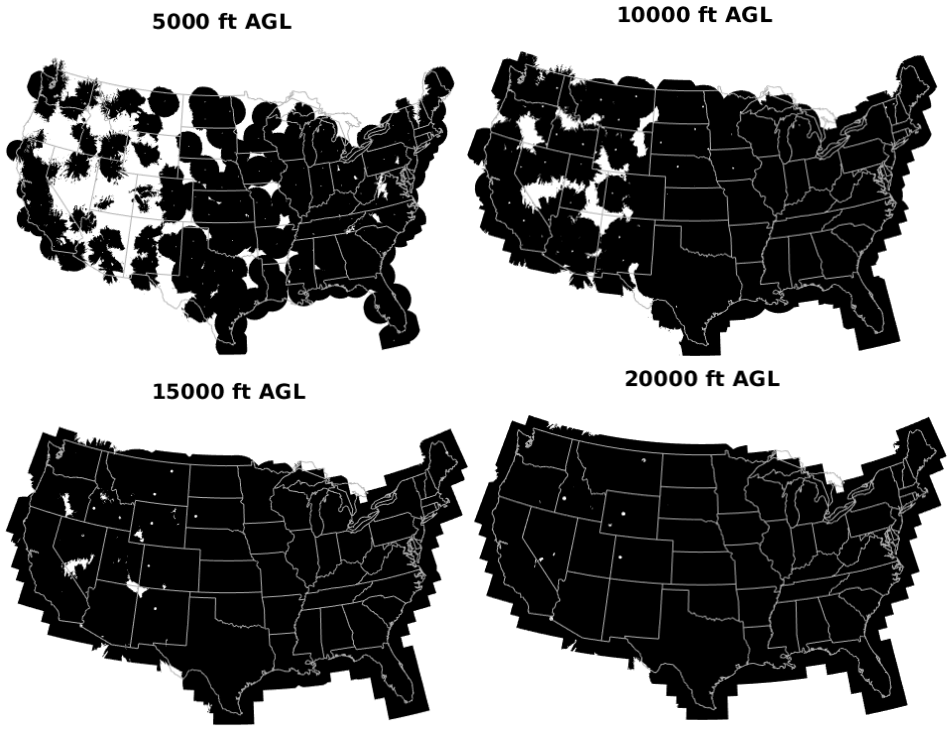

Figure 2-3. Coverage provided by the WSR-88D network at 5000 ft, 10,000 ft, 15,000 ft, and 20,000 ft AGL .

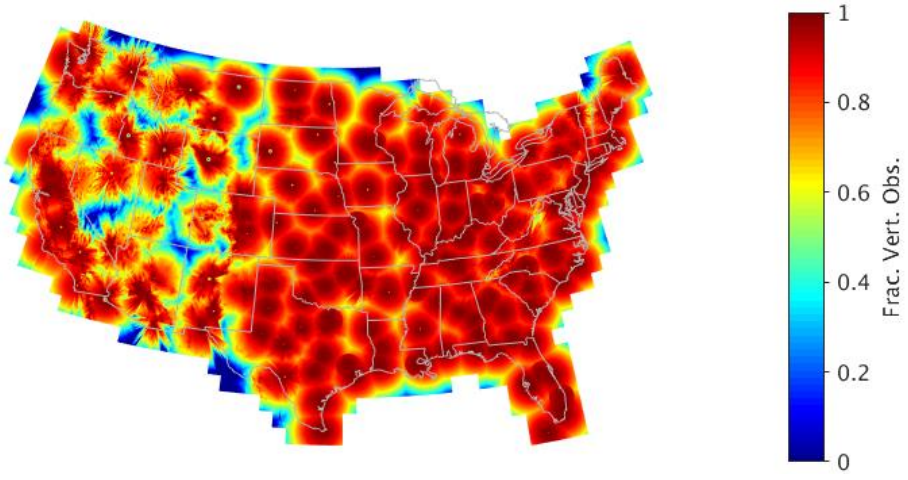

Figure 2-4. Fraction of vertical volume observed between 0 and 20 kft AGL by current CONUS WSR-88Ds and TDWRs.

We also considered the cross-radial horizontal resolution (CHR). This parameter is important for detection of tornadic velocity couplets (Wood and Brown 1997; Brown et al. 2002; Brown and Wood 2012). Along-range horizontal resolution is also a factor but is not an interesting metric, because it is a constant value everywhere for monostatic radars. Roughly speaking, CHR is angular resolution (in radians) multiplied by range. Angular resolution is dependent on the antenna beamwidth and the dwell size (Zrnic and Doviak 1976). Although the TDWR's beamwidth is about half that of the WSR-88D's (0.55° vs. 1°), because its sampling interval is 1°, the effective angular resolution of the two systems are not very different. Currently, the WSR-88D has a so-called "superresolution" mode that outputs data at overlapping 0.5° intervals, but the effective angular resolution is still ~1° based on the data window and the beamwidth (Torres and Curtis 2006). Therefore, we approximated the angular resolution of both systems as 1°. The resulting CHR is, thus, functionally the same as the distance-from-radar metric for the current radars. Terrain blockage was not factored in, because that is elevation angle dependent, and we did not want to pick a particular angle for this metric. Figure 2-5 maps CHR over the CONUS for the combined WSR-88D and TDWR networks. Future radars, however, could have very different angular resolutions, e.g., a dense network of broad-beam systems (Brotzge et al. 2010), or even angle-dependent resolution for fixed planar phased arrays (Brown and Wood 2012), which may make CHR a more meaningful performance yardstick.

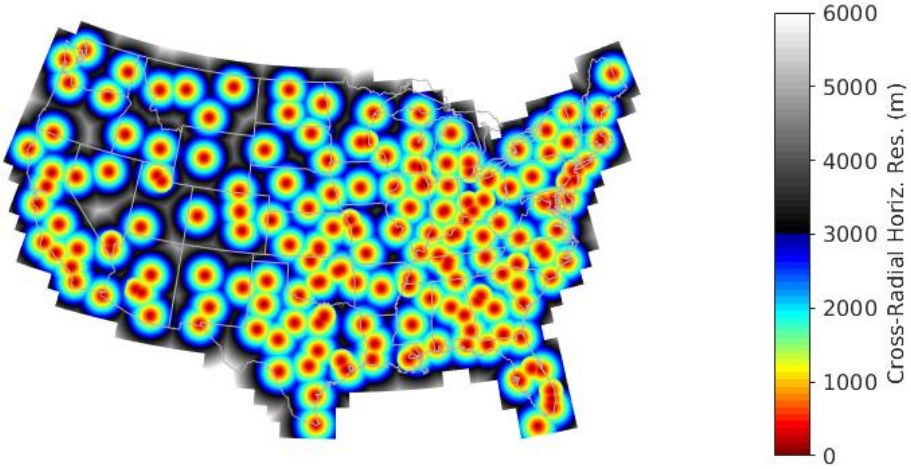

Figure 2-5. Cross-radial horizontal resolution for current CONUS WSR-88Ds and TDWRs.

2.3 MODEL DEVELOPMENT

Tornado warnings are expected to benefit society by allowing people to shelter in advance of impact, thereby reducing casualties. This intuitive causal chain has been proven empirically, at least for the case of injuries (Simmons and Sutter 2008); fatalities are such rare events that it is difficult to achieve statistically significant results for them. Little can be done to protect property at warning time scales, so we only considered casualty reduction in our model. At the same time, there is a cost incurred for those taking

shelter based on the loss of work and personal time. If false alarms can be decreased, some of this cost could be recouped (section 2.3.8).

Better Doppler weather radar coverage should contribute to tornado casualty reduction by improving tornado warning performance. It may also lower sheltering cost by decreasing false alarms. Our benefit model combined all of these effects to output a monetized cost given an arbitrary weather radar network as input (Figure 2-6).

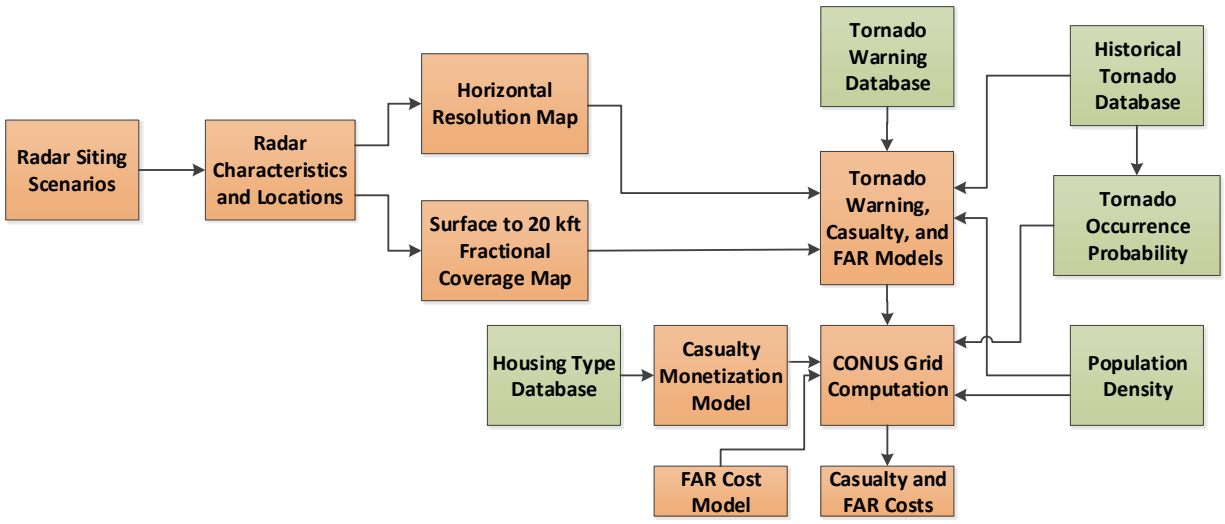

Figure 2-6. Block diagram of weather radar network benefit model for tornado warnings.

2.3.1 Detection Probability Dependence on Radar Coverage

A five-year (2000–2004) study (Brotzge and Erickson 2010) showed that the fraction of tornadoes without warning increased with distance from radar, which implies that better radar coverage improves tornado warning performance. We performed our own analysis using NWS tornado warning data, extending the analysis period. National deployment of operational WSR-88Ds was completed in late 1997. Therefore, we set the analysis period to be between 1 January 1998 and 31 December 2018. However, after 1998, two new WSR-88D sites were added—Evansville, Indiana (operational January 2003) and Langley Hill, Washington (installed September 2011). Furthermore, the TDWR Supplemental Product Generator (SPG) deployment (Istok et al. 2009a), which enabled TDWR data access by NWS forecasters, was finished in late 2008. Thus, to account for these radar network changes, we generated four sets of FVO and CHR maps: (1) Prior to the Evansville WSR-88D installation, (2) after the Evansville addition but before the

TDWR SPG deployment, (3) post-TDWR SPG but before the Langley Hill WSR-88D installation, and (4) after the Langley Hill deployment. We did not discriminate between the periods before and after the WSR-88D dual-polarization upgrade, since overall tornado warning statistics did not improve post-upgrade in our analysis (Figure 2-7). The mean tornado fraction warned prior to the start of the dual-polarization deployment but after the switch to storm-based warnings (October 2007 to February 2011) was 0.74, whereas it was 0.63 after the completion of the upgrade (June 2013 to December 2018). This methodology is not perfectly accurate, as we did not take into account the exact periods of radar down times, variations in volume scanning strategies, etc., but the expansion of the analyzed database to twenty years helped suppress the noise level of these minor errors relative to the desired signal.

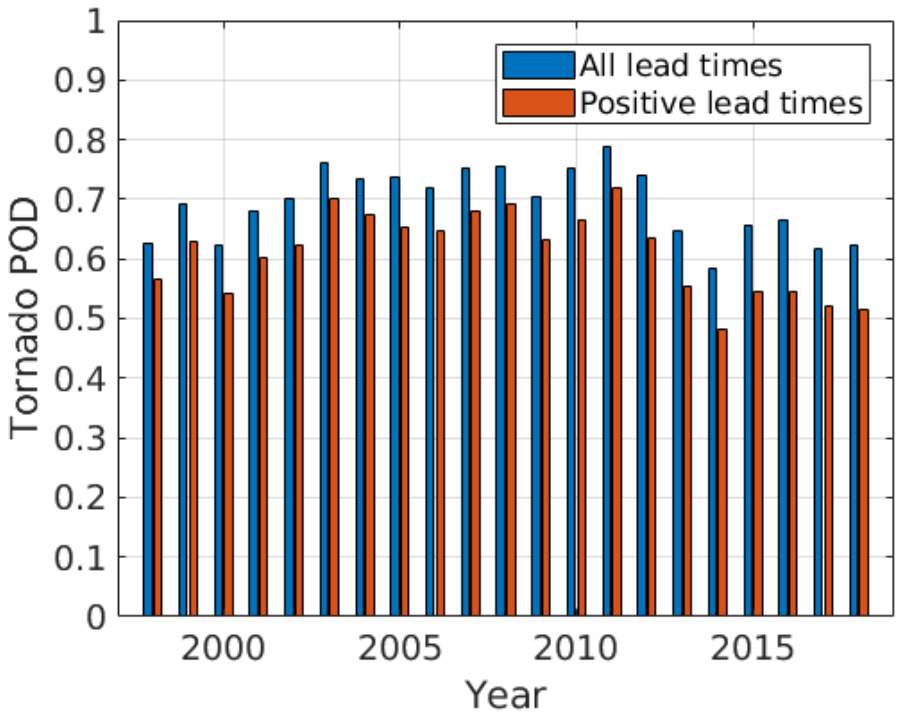

Figure 2-7. CONUS tornado detection probability by year.

Tornado event data were downloaded from the storm events database (https://www.ncdc.noaa.gov/stormevents/) of NOAA's National Center for Environmental Information. Tornado warning data were obtained from the Iowa Environmental Mesonet NWS Watch/Warnings archive (https://mesonet.agron.iastate.edu/request/gis/watchwarn.phtml). A warning was deemed to be a hit if any portion of the tornado path was inside the area enclosed by the warning latitude-longitude coordinates and if any part of the tornado existence period overlapped the warning valid interval; otherwise, the warning

was classified as a false alarm. For a hit, the lead time was calculated as the tornado start time minus the initial time of warning issuance. Multiple warnings for one storm were treated separately. For the remainder of the paper, we will refer to the fraction of tornadoes with warning as the probability of detection (POD), which is the more commonly used term. The number of tornadoes and POD during the analysis period, parsed by Enhanced Fujita (EF) scale number, are given in Table 2-1.

Table 2-1 CONUS Tornado Warning Statistics for Analysis Period

EF#	0	1	2	3	4	5
Tornado count	16 517	8789	2632	790	171	19
POD (all lead times)	0.66	0.70	0.84	0.95	0.98	1.0
POD (positive lead times only)	0.59	0.61	0.74	0.87	0.92	1.0

Prior to February 1, 2007, the original Fujita scale was used to rate tornadoes. With a far greater number of damage indicators used, the EF scale is agreed to be a more accurate and consistent estimator of tornado strength. Although carefully designed to minimize discontinuity in the historical tornado database, there may still be some small statistical differences between the old and new scales, such as shifts in the relative distributions between strength categories (Edwards and Brooks 2010), which could potentially affect our regression results.

For each tornado event, FVO and CHR at the start-of-tornado location were recorded. Based on similarities in POD statistics, and also to increase the number of samples per category for the high-EF cases, we then computed POD vs. FVO and CHR for EF0–1, EF2, and EF3–5. For these calculations, FVO was binned into the following intervals: [0, 0.3], (0.3, 0.6], (0.6, 0.7], (0.7, 0.8], (0.8, 0.9], and (0.9, 1], while CHR (in meters) was binned into: [0 500], (500, 1000], (1000, 1500], (1500, 2000], (2000, 2500], and (2500, ∞).

Figure 2-8 shows POD vs. FVO for EF0–1, EF2, and EF3–5, where warnings with any lead time (including zero and negative values) are considered valid. The argument in favor of this interpretation is that even if a tornado touches down before the warning issuance time, as long as the warning is issued before the end of the event, people further down the track have a chance to shelter before impact. The plotted abscissa values are the means of the binned FVO data, not the center of the bins. The horizontal error bars are ±1.96 times the FVO standard deviation divided by the square-root of the number of data points. The vertical error bars are ±1.96 times the standard error for proportional data (the computed PODs) divided by the square-root of the number of data points. These bars indicate the 95% confidence intervals

in both dimensions. A minimum of four data points per bin were required for inclusion in the plots, which eliminated low-FVO points with increasing EF number.

Figure 2-9 shows POD vs. FVO for EF0–1, EF2, and EF3–5, where only warnings with positive lead

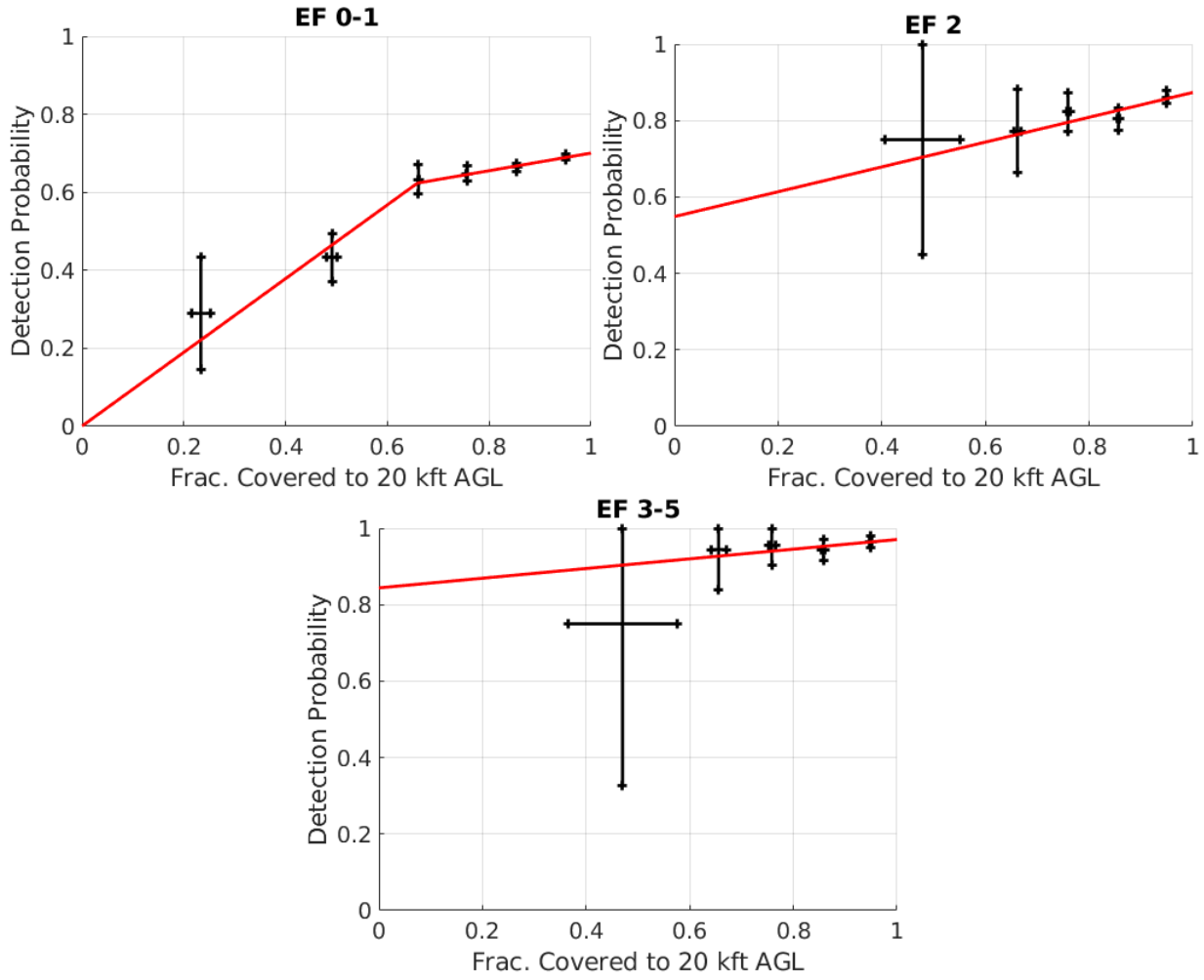

Figure 2-8. Tornado detection probability vs. fraction of vertical volume covered by radar from surface to 20 kft AGL: (top left) EF0 and EF1, (top right) EF2, and (bottom) EF3, EF4, and EF5. Presence of warning with any lead time is considered a detection. Solid red lines are least-squares linear fits to the data.

times are considered detections. The main effect of excluding zero and negative lead times was to lower the POD values as expected, but the general trends are quite similar in Figures 2-7 and 2-8. That is, POD increases with FVO for all EF categories. This is a key result, as it associates improvement in tornado warning performance to better radar coverage. We modeled these dependencies with least-squares straight

line fits to the data with input uncertainty in two dimensions using the Numerical Recipes function fitexy (Press et al. 1992). Results of the fitting are listed in Table 2-2, where a is the y intercept, b is the slope, σ_a is the standard deviation of a, σ_b is the standard deviation of b, χ^2 is the final chi-squared value, and Q is the goodness-of-fit probability. The slopes are positive; they remain positive within the errors except for the EF3–5 cases, which have much fewer data points than the other categories. The dashed red line in the EF0–1 plot in Figure 2-9 will be explained in section 2.3.6. The decision of whether to use the all-lead-time or positive-lead-time-only fits in our model will be discussed in section 2.3.4.

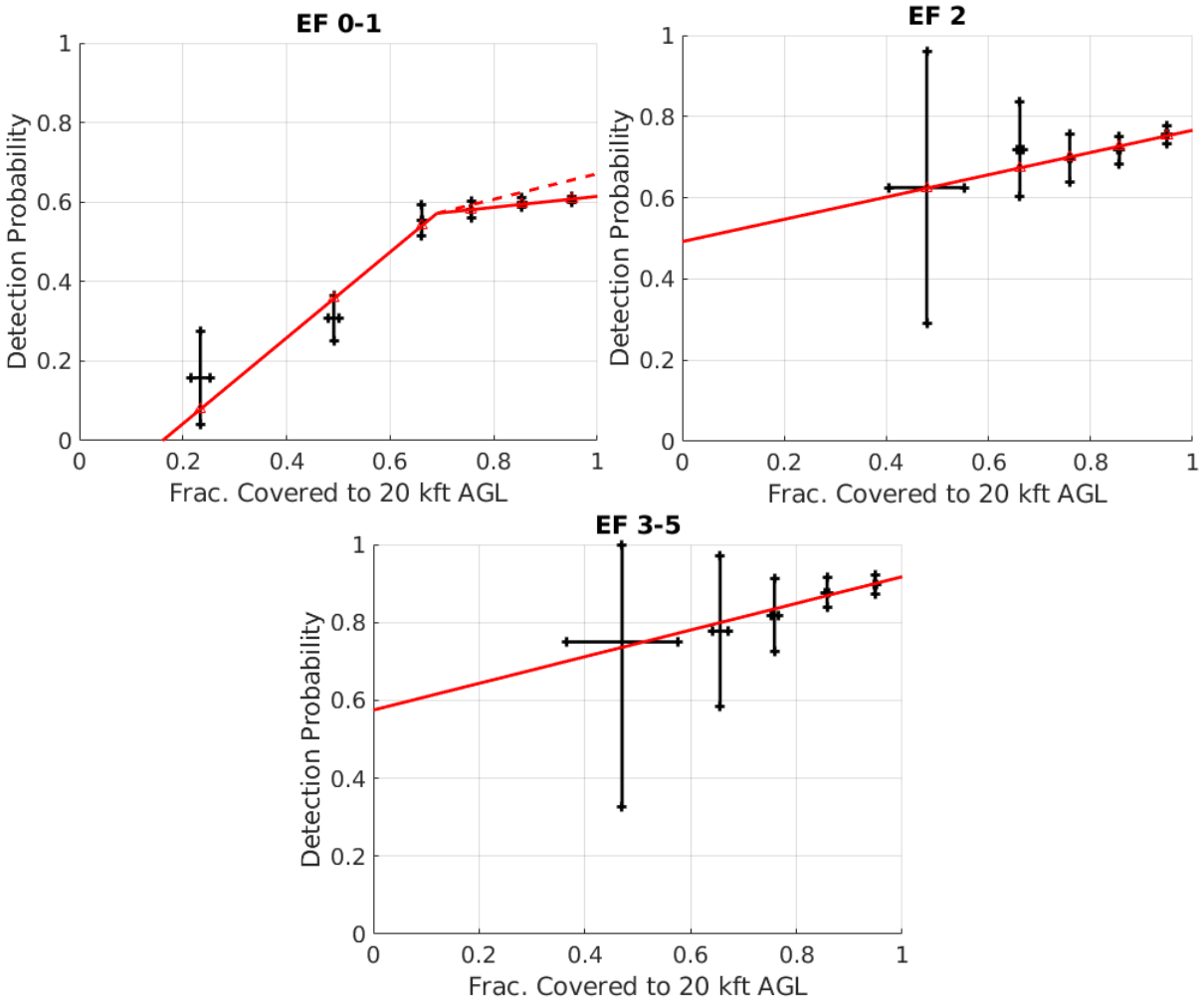

Figure 2-9. Same as Figure 2-8, except only warnings with positive lead times are considered detections. Dashed red line corresponds to rapid scanning radar case.

Table 2-2 POD vs. FVO Linear Fit Results

EF# group	0–1		2	3–5
Segment	Low FVO	High FVO	All FVO	All FVO
All lead times				
a (y intercept)	0.00	0.48	0.55	0.84
b (slope)	0.94	0.23	0.32	0.13
σ_a	0.18	0.07	0.18	0.18
σ_b	0.30	0.08	0.24	0.19
χ^2	0.51	0.20	0.99	0.36
Q	0.48	0.90	0.80	0.95
Positive lead times only				
a (y intercept)	-0.17	0.48	0.49	0.58
b (slope)	1.1	0.14	0.27	0.34
σ_a	0.15	0.08	0.21	0.29
σ_b	0.26	0.09	0.27	0.38
χ^2	1.3	0.27	0.26	0.10
Q	0.26	0.87	0.97	0.99

The dependence of POD on CHR was more problematic, as POD did not decrease monotonically with increase in CHR. Figure 2-10 shows the results for all EF categories combined. Since CHR is proportional to distance from the nearest radar, the decrease in POD at close range may be at least partly due to the negative impact of the cone of silence. This type of cross-contamination of effects is undesirable, since future radar systems could have a significantly smaller cone of silence and a CHR-POD relationship based mostly on WSR-88D data may not hold. Therefore, we excluded CHR as a radar performance metric from the POD dependency model.

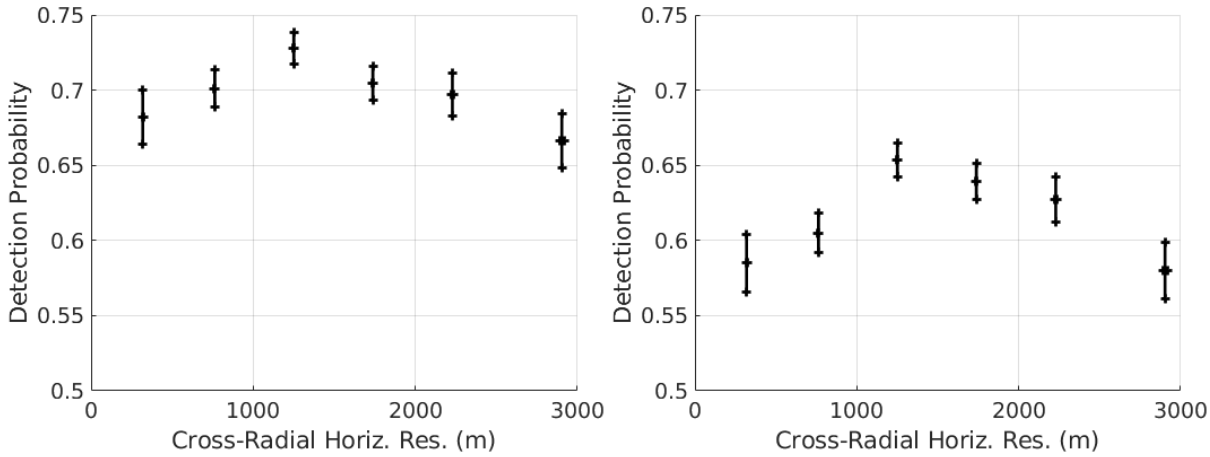

Figure 2-10. Tornado detection probability vs. cross-radial horizontal resolution of radar observations for detection based on (left) all warning lead times and (right) positive lead times only.

2.3.2 False Alarm Ratio Dependence on Radar Coverage

Tornado warning false alarm ratio (FAR) depends on many factors, e.g., time of day, population density, and tornado occurrence frequency. An earlier five-year study (2000–2004) showed FAR more-or-less constant with distance from radar up to ~150 km, but then decreasing at farther ranges (Brotzge et al. 2011). Taken at face value, this meant that improving radar coverage would not lower FAR, and might even raise the overall number of false alarms. It is also possible that lower FAR (and lower POD) might result from forecasters' reluctance to issue warnings where they know radar coverage is poor. Thus, we revisited this study using the FVO and CHR radar coverage metrics instead of distance from radar, and expanded the database period as we did for the POD dependency analysis in section 2.3.1.

An important point about the database is that operational NWS tornado warnings switched from a county-based to a storm-based polygon area definition on 1 October 2007. This transition made a large difference in the warning statistics as seen in Table 2-3, with the mean warning area shrinking to 40% of the former mean area. Because the analysis of FAR vs. the radar coverage metrics involved computation of the average coverage parameters over the warning area, the change to storm-based warning resulted in much sharper relationships. This was in contrast to the POD analysis of section 2.3.1, which used the location of the tornado with the radar coverage values, not the warning area. Therefore, in this section, we only used the database period 1 October 2007 to 31 December 2018.

Table 2-3 Tornado Warning Statistics Before and After Switch to Storm-based Warnings

Period	1998-1-1 to 2007-9-30	2007-10-1 to 2018-12-31
Warning count	33 814	25 290
Mean warning area	2370 km^2	953 km^2
FAR	0.763	0.722

For the FAR vs. radar coverage calculations, FVO was binned into the following intervals: [0, 0.3], (0.3, 0.4], (0.4, 0.7], (0.7, 0.8], (0.8, 0.9], and (0.9, 1], while CHR (in meters) was binned into: [0 700], (700, 1400], (1400, 2100], (2100, 2800], (2800, 3500], and (3500, ∞). Limits were adjusted to spread out the data distribution more evenly among bins. The results and subsequent linear fits are plotted in Figure 2-11 (FAR vs. FVO) and Figure 2-12 (FAR vs. CHR); the fitting procedure was the same as for Figures 2-8 and 2-9 as explained in section 2.3.1. For Figure 2-12, the line fit excluded the rightmost data point, and the FAR was capped at 0.76 as shown by the horizontal red line, a piecewise linear approximation of what appears to be a saturation curve type of behavior. The dashed red line will be explained in section 2.3.6.

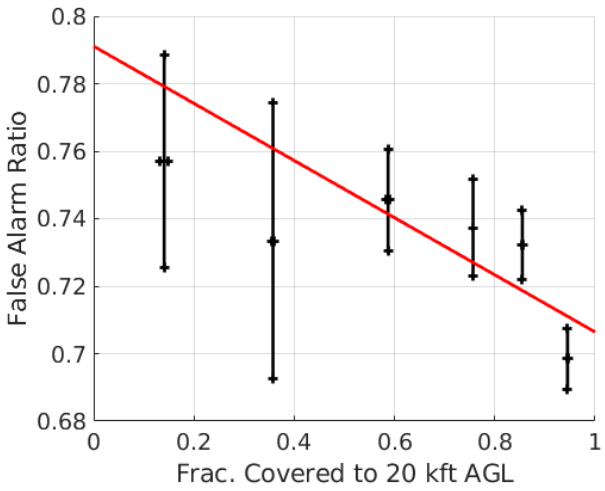

Figure 2-11. Tornado warning false alarm ratio vs. fraction of vertical volume covered by radar from surface to 20 kft AGL. Red line is a least-squares linear fit to the data.

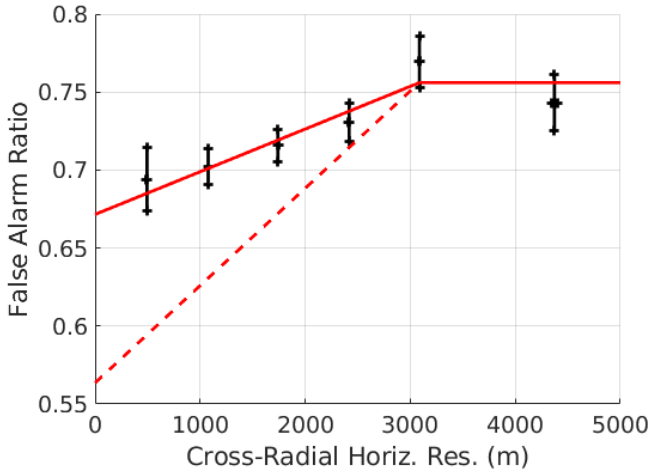

Figure 2-12. Tornado warning false alarm ratio vs. mean cross-radial horizontal resolution of radar observations. Sloped solid red line is a least-squares linear fit to first five data points. Dashed red line corresponds to rapid scanning radar case, which will be explained in section 2.3.6.

Curiously, in this case, FAR vs. CHR yielded the better fit. Coefficients and fitting statistics are given in Table 2-4. In an attempt to optimally combine CHR and FVO in the FAR-radar coverage model, we tried weighted means of the two linear relationships and compared the resulting errors (mean-squared sums of the difference between model and data). The smallest error was achieved with zero weighting on the FVO relationship. Thus, only the FAR-CHR relation was used in our model.

Table 2-4 FAR vs. Radar Coverage Parameter Linear Fit Results

Parameter	FVO	CHR
a (y intercept)	0.79	0.67
b (slope)	-0.085	2.7×10^{-5} m^{-1}
σ_a	0.026	0.015
σ_b	0.033	7.9×10^{-6} m^{-1}
χ^2	5.3	1.3
Q	0.26	0.72

2.3.3 Warning Lead Time Dependence on Radar Coverage

Since we were able to establish significant links between radar coverage parameters and tornado warning POD and FAR, one might also hope to find a statistically meaningful relationship between the former and tornado warning lead time. Unfortunately, data analysis did not yield such a connection. Figure 2-13 shows 2D histograms of warning lead time vs. FVO and CHR. There was no apparent trend in either case, and the linear regression fits shown had slopes that were the opposite signs of what one would expect (positive for FVO and negative for CHR). In any case, the goodness-of-fits were poor, with R^2 values less than 0.005 in both cases. Excluding negative lead times and parsing the data by EF number also produced similarly inconclusive results. This is consistent with past reports (Brotzge and Erickson 2009). Therefore, we could not include tornado warning lead time enhancement as a beneficiary of improved radar coverage.

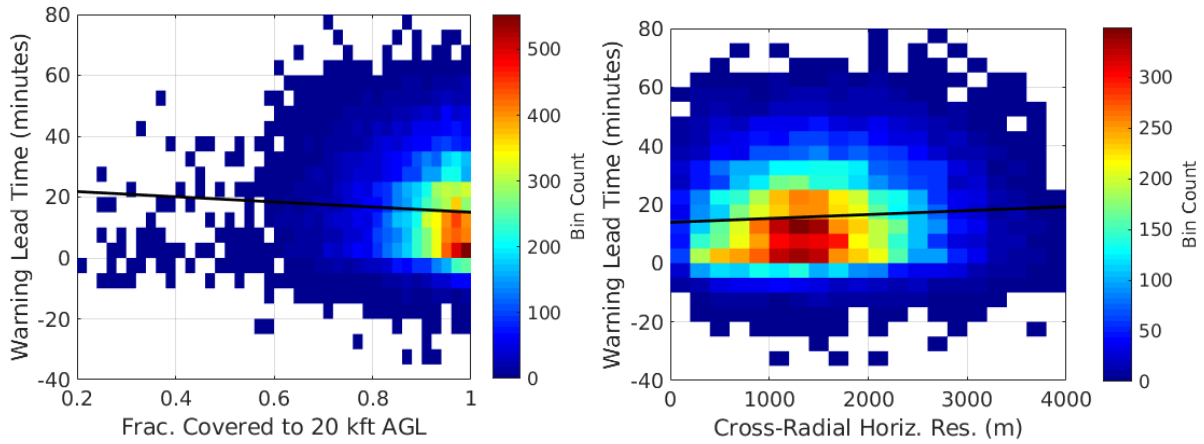

Figure 2-13. 2D histograms of tornado warning lead time vs. (left) FVO and (right) CHR. The black lines are linear regression fits to the data.

2.3.4 Casualty Dependence on Tornado Warning

Now that we have established models for dependency of tornado warning performance on radar coverage, we move on to discuss casualty dependence on tornado warnings. Tornado casualty rate is positively correlated with surface dissipation energy, population density, fraction of mobile homes in housing stock, and FAR (Ashley 2007; Simmons and Sutter 2009; Fricker et al. 2017). The dependence on historical FAR may be due to "the boy who cried wolf" effect, where residents used to a high FAR are less likely to heed warnings seriously and take shelter (LeClerc and Joslyn 2015); research on this topic, however, has yielded mixed results (Lim et al. 2019). Tornado casualty rate is negatively correlated with the presence of tornado warnings, as expected; when a tornado warning is correctly issued, one intuits that lead time should also be negatively correlated with casualty, but this has not been established, as the

dependence of casualty rate on lead time is not monotonic (Simmons and Sutter 2008). We include a lead time variable to see if a meaningful relationship can be established. Time-based variables like season and time of day were also shown to be significant predictors of casualty rate, but these are not factors that we can use in our time-independent cost generation model, so we did not consider them.

Since casualty is a counting variable and its statistical distribution is overspread, we followed the earlier studies in assuming a negative binomial distribution model,

$$C \sim \text{NegBin}(\mu, \theta) \,, \tag{2-1}$$

where C is conditional casualty count, μ is the distribution mean, and θ is the dispersion parameter (Simmons and Sutter 2008; Fricker et al. 2017). Our regression model is expressed as

$$\ln \mu = \alpha \ln P_T + \beta \ln S + \gamma M + \delta F_0 + \varepsilon W + \zeta T + k \,, \tag{2-2}$$

where P_T is population inside the tornado path, S is tornado surface dissipation energy density, M is fraction of P_T residing in mobile homes, recreational vehicles, and vans, F_0 is mean historical FAR inside the tornado path, W is warning presence (0 for absent, 1 for present), T is the warning lead time (in seconds), k is the intercept constant, and α, β, γ, δ, ε, and ζ are the regression coefficients. A warning was defined to be present if there was a lead time (positive or negative). For lead time input data, in order to have a logical cutoff for the minimum value, we set all instances of no warning and negative lead times to zero. The tornado surface dissipation energy density is (Fricker et al. 2017)

$$S = \rho \sum_{m=0}^{5} w_m v_m^3 \,, \tag{2-3}$$

where ρ is the air density (assumed to be 1 kg m^{-3}), v is the midpoint wind speed for each EF value m, and w is the corresponding fraction of the path area. Because there is no upper bound speed for EF5, we set a midpoint of 97 m s^{-1} following Fricker et al. (2017). Path area fractions are not given in the tornado database, so mean w_m values were taken from Table 3-1 of Ramsdell and Rishel (2007).

In Equation 2-2 it is not intuitively obvious that population should be used instead of population density or that dissipation energy density should be used instead of dissipation energy; Fricker et al. (2017) opted for population density and dissipation energy. Both terms should not be posed as density, since that would omit the important tornado path area factor. We chose to use the combination that gave the best regression fit, and that was dissipation energy density and population.

Recently, Elsner et al. (2018) proposed a nonlinear casualty model in which the casualty elasticity with respect to energy dissipation increases with population density. To account for this hypothesized effect, they added a multiplicative term (log of population density times log of energy dissipation) to their regression equation. We tried this scheme with our data, but the results showed that the fit statistics were much worse with the added term. Therefore, we opted to stay with the linear model.

We did not separate casualties into fatalities and injuries at this stage, as the former is merely the extreme end case of the latter. By combining the two groups, we avoided the problem of extremely sparse statistics for fatalities. Only direct casualties were included to tighten the causal relationship between the tornado and its impact on people. In the monetization stage (section 2.3.5), we parsed the model results into fatalities and two types of injuries.

For population data, we obtained gridded population density from the Center for International Earth Science Information Network (CIESIN 2017). The latitude-longitude resolution of this data matched our model grid spacing of 30 arcsec. Data were available for the years 2000, 2005, 2010, 2015, and 2020 (projected). The 2015 CONUS population density is plotted in Figure 2-14; a base-ten log scale is used to visually compress the large dynamic range around urban regions. For 1998–1999 we used the 2000 data, and for other years we linearly interpolated as needed between the available years.

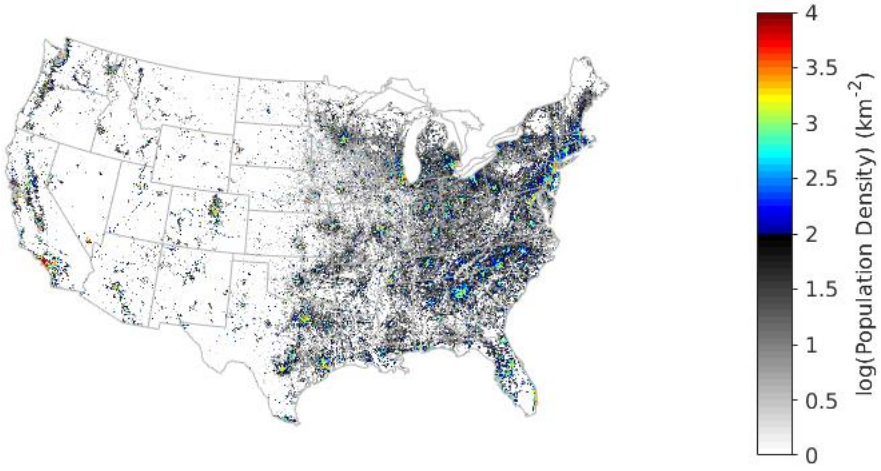

Figure 2-14. CONUS population density (logarithmic scale) in 2015.

Mobile housing statistics were pulled from the American Community Survey database for 2015 (USCB 2016) and the Decennial Census for 2000 (Manson et al. 2018). The population in housing units

were broken down by building structure categories, one of which was "mobile home." We grouped this together with the much smaller "boat, RV, van, etc." category to arrive at our mobile housing population. The highest spatial resolution data available (block group level) were normalized by the total population in each block group to yield the fraction of population in mobile housing. This data set was then sampled and mapped to our latitude-longitude grid to generate the CONUS maps. In the regression analysis, the 2000 map was used for 1998–2000, the 2015 map (Figure 2-15) was used for 2015–2018, and linearly interpolated maps (between 2000 and 2015) were used for the years 2001–2016. Although only 5.8% of the national population lives in mobile housing, because they are prevalent in rural regions, disproportionately large areas of the country have significantly higher fractions.

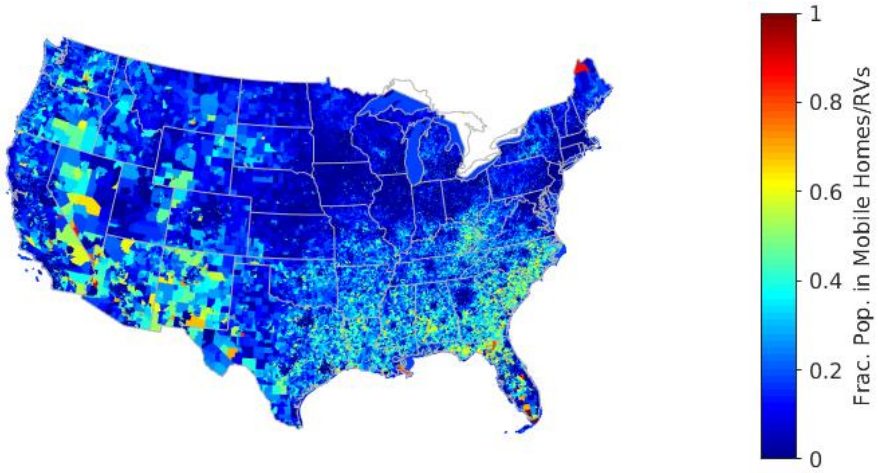

Figure 2-15. Fraction of population residing in mobile homes and RVs in 2015.

From the tornado warning data, we computed CONUS maps of historical FAR on our model grid for the periods before and after storm-based warnings (Figure 2-16). Areas with no data were dropped from the regression analysis.

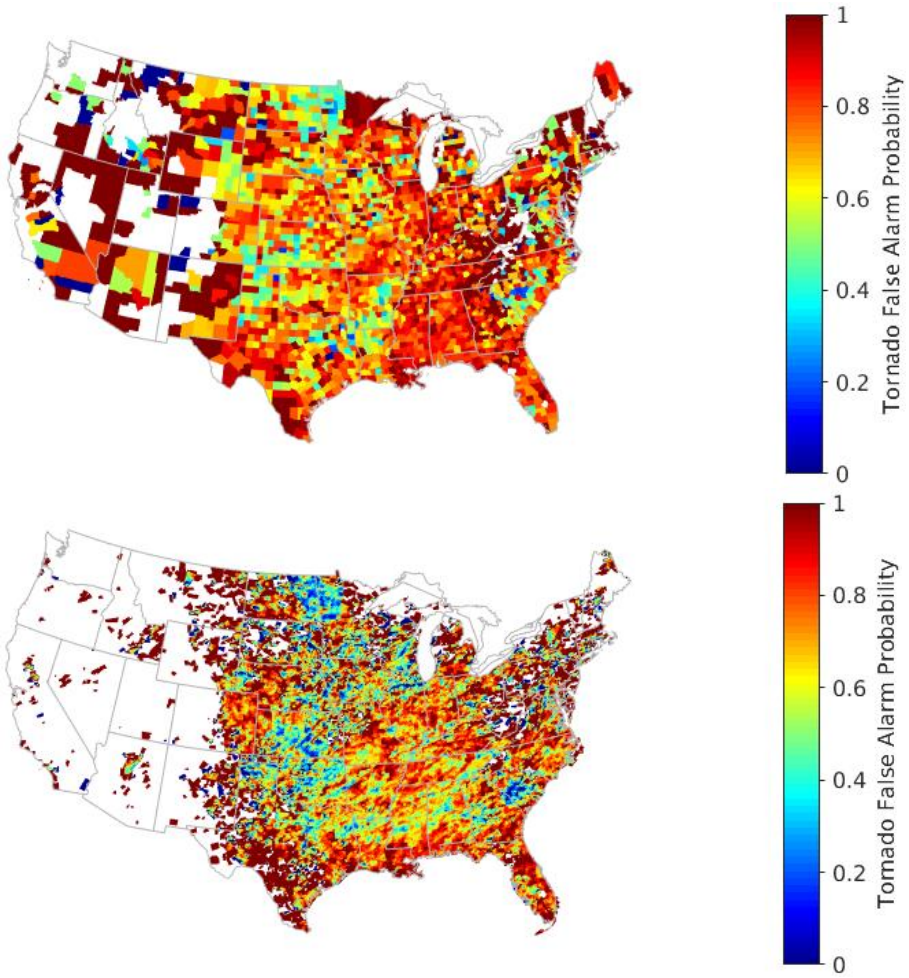

Figure 2-16. Historical FAR for (top) 1 January 1998 to 30 September 2007, in the county-based warning era, and (bottom) 1 October 2007 to 31 December 2018, in the storm-based warning era.

We used the function glm.nb from the open statistical analysis software package R (R Core Team 2018) for the negative binomial regression analysis. The results are given in the top half of Table 2-5. All coefficients estimates had the expected signs, i.e., mean casualty per tornado was positively correlated with population, tornado dissipation energy, and FAR, and it was negatively correlated with the presence of tornado warning; casualty rate was also negatively correlated with warning lead time. The coefficient signs were constant within the standard errors, and the *z* statistics (Wald test) showed that all coefficient estimates were significant at a better than 9×10^{-11} level, except for ζ, the lead time coefficient for results computed from the entire time period of our database. (The *z* value is the estimate divided by the standard error, and the probability of $|z|$ exceedance is rejection of the null hypothesis at that level.) Furthermore, comparing models with and without each variable through degree-of-freedom chi-square tests indicated that every

variable was a statistically significant predictor of casualty rate. Application of Equation 2-2 with the estimated coefficients to the same input data yielded a casualty count of 23,501 compared to the actual count of 23 675, which is a difference of only 0.7%. According to this model, the presence of a tornado warning reduces casualty by 40%.

Table 2-5 Tornado Casualty Model Regression Results

Data Period	Coefficient	Estimate	Std. Error	*z*	Pr (> |*z*|)
1998-1-1 to 2018-12-31	α (log. population)	0.315	0.0121	26.0	$< 2 \times 10^{-16}$
	β (log. energy density)	6.04	0.128	47.2	$< 2 \times 10^{-16}$
	γ (mobile home fraction)	1.70	0.196	8.69	$< 2 \times 10^{-16}$
	δ (historical FAR)	1.24	0.147	8.44	$< 2 \times 10^{-16}$
	ε (warning presence)	-0.504	0.0778	-6.48	9×10^{-11}
	ζ (lead time)	-1.04×10^{-4}	4.20×10^{-5}	-2.48	0.01
	k (intercept constant)	-68.2	1.38	-49.5	$< 2 \times 10^{-16}$
	θ (dispersion parameter)	0.142	0.00466	N/A	N/A
2007-10-1 to 2018-12-31	α (log. population)	0.340	0.0176	19.4	$< 2 \times 10^{-16}$
	β (log. energy density)	6.09	0.180	33.8	$< 2 \times 10^{-16}$
	γ (mobile home fraction)	1.32	0.274	4.83	1×10^{-6}
	δ (historical FAR)	1.17	0.197	5.93	3×10^{-9}
	ε (warning presence)	-0.352	0.110	-3.19	0.001
	ζ (lead time)	-1.33×10^{-5}	5.90×10^{-5}	-0.225	0.8
	k (intercept constant)	-70.9	2.54	-27.9	$< 2 \times 10^{-16}$
	θ (dispersion parameter)	0.116	0.00695	N/A	N/A

Regression analysis was performed on all data as well as data since the implementation of storm-based warnings (bottom half of Table 2-5). Comparison of Table 2-5 top- and bottom-half values shows that the results were quite robust relative to this data segmentation, except for the lead time variable. Since the statistical fits are better with the larger data set, henceforth we will only show results using the full data set.

Since warning lead time was not a statistically reliable variable in the full regression equation, we tried removing it. Table 2-6 gives the corresponding regression results. The coefficient estimates hardly change and a better statistical fit is obtained for the warning presence variable.

Table 2-6 Tornado Casualty Model Regression Results without Lead Time Variable

Coefficient	Estimate	Std. error	*z*	Pr (> |*z*|)
α (log. population)	0.315	0.0121	26.0	$< 2 \times 10^{-16}$
β (log. energy density)	6.02	0.127	47.3	$< 2 \times 10^{-16}$
γ (mobile home fraction)	1.68	0.196	8.58	$< 2 \times 10^{-16}$
δ (historical FAR)	1.25	0.147	8.48	$< 2 \times 10^{-16}$
ε (warning presence)	-0.598	0.0677	-8.83	$< 2 \times 10^{-16}$
k (intercept constant)	-68.0	1.37	-49.6	$< 2 \times 10^{-16}$
θ (dispersion parameter)	0.142	0.00465	N/A	N/A

We also tried keeping the lead time variable, but omitting the warning presence variable. The results are given in Table 2-7. In this case, lead time variable yielded a statistically reliable regression fit. Moreover, the negative coefficient estimate indicated that increased lead time resulted in reduced casualty rate as expected, and the sign was consistent within the standard error bounds. It may be that including both warning presence and lead time in the regression created an "interference" condition, because they are highly correlated variables. In any case, we could not justifiably keep both variables in our regression model.

Table 2-7 Tornado Casualty Model Regression Results without Warning Presence Variable

Coefficient	Estimate	Std. error	*z*	Pr (> |*z*|)
α (log. population)	0.306	0.0121	25.4	$< 2 \times 10^{-16}$
β (log. energy density)	5.96	0.127	47.0	$< 2 \times 10^{-16}$
γ (mobile home fraction)	1.63	0.196	8.29	$< 2 \times 10^{-16}$
δ (historical FAR)	1.44	0.145	9.92	$< 2 \times 10^{-16}$
ζ (lead time)	-2.33×10^{-4}	3.70×10^{-5}	-6.31	3×10^{-10}
k (intercept constant)	-67.7	1.37	-49.4	$< 2 \times 10^{-16}$
θ (dispersion parameter)	0.141	0.00463	N/A	N/A

Hence, we were left with a dilemma. On one hand, because the radar coverage parameters (FVO and CHR) had a clear link to tornado warning POD but had no correlation with lead time, we preferred to keep the warning presence variable in the casualty regression model. On the other hand, since increasing warning lead time is a high priority for the NWS, we wished to use the newly established statistically meaningful relationship between it and casualty reduction to generate quantitative benefits. We overcame this quandary by choosing to include only lead time in the casualty model. In the model casualty computation over the geospatial grid, two separate terms were calculated—one with mean positive lead times (warning present) and the other with zero lead time (warning absent). The terms were multiplied by the probabilities of warning and no warning, respectively, then summed. This process is explained in section 2.3.7. In order to keep this procedure consistent, we had to define warning POD as being restricted to warnings with positive lead times. (c.f. last paragraph of section 2.3.1).

2.3.5 Casualty Monetization

In benefit studies like this one, the value of a statistical life (VSL) is often used to monetize casualties. VSL is an estimate of one's willingness to pay for small reductions in mortality risks. We adopted the Department of Transportation's guidance (DOT 2016), which called for a VSL of $9.6M in 2015 dollars. To adjust the value to 2019 dollars, we employed the DOT's formula,

$$\mathrm{VSL_T} = \mathrm{VSL_0}\,\frac{\mathrm{CPI_T}}{\mathrm{CPI_0}}\left(\frac{\mathrm{MUWE_T}}{\mathrm{MUWE_0}}\right)^{q}, \tag{2-4}$$

where CPI is the consumer price index, MUWE is the median usual weekly earnings, q is income elasticity, and the subscripts T and 0 denote updated base year and original base year. From the U.S. Bureau of Labor Statistics (BLS) online database, we obtained $\mathrm{CPI_T/CPI_0}$ = 1.08 (https://www.bls.gov/data/inflation_calculator.htm) for a baseline of January 2015 and updated time of January 2019, and $\mathrm{MUWE_T/MUWE_0}$ = 1.12 (https://www.bls.gov/cps/cpswktabs.htm) for a baseline of 2015 first quarter and updated time of 2019 first quarter. With the DOT's estimate of q = 1, we got a 2019 VSL of $11.6M.

As discussed in section 2.3.4, our casualty regression model did not differentiate between fatalities and injuries. To parse the model output into the two types of casualty, we relied on the strong relationship between EF category and relative proportions of casualty types computed from the tornado database. Table 2-8 gives the mean fraction of casualties that are fatalities vs. EF number.

Table 2-8 Mean CONUS Tornado Statistics vs. EF Number

EF#	Fatality fraction	Path area (km^2)	Surface dissipation energy density (GW km^{-2})
0	0.027	0.0279	37.6
1	0.049	0.353	48.2
2	0.053	1.67	64.8
3	0.066	5.88	85.2
4	0.067	11.9	96.8
5	0.15	29.3	114

Injuries can be monetized as fractions of VSL. To do this, we referenced a Federal Emergency Management Administration (FEMA) tornado safe room benefit study (FEMA 2009). Their formulation specified injuries requiring hospitalization as level 4 (severe) and injuries that led to professional treatment and immediate release as level 2 (moderate). The latest DOT guidance sets the level 4 injury cost at 0.266 × VSL and level 2 injury cost at 0.047 × VSL (DOT 2016). In 2019 dollars, these costs are $3.09M and $0.545M, respectively. All estimated casualty costs are compiled by type in Table 2-9.

Table 2-9 Casualty Cost by Type

Casualty type	Cost ($M)
Fatality	11.6
Injury (hospitalized)	3.09
Injury (treated and released)	0.545

The historical tornado database does not differentiate injuries by severity. Thus, we needed another way to generate model output for injuries requiring hospitalization versus those that are treated and released. Fortunately, the FEMA report connected the probability of injury levels to tornado EF class and building type. We simplified the building categories to two (mobile housing and other) to match the gridded fraction of population in housing data that we obtained for the regression analysis. For the "other" category, we averaged the FEMA table values for one- and two-family residences and institutional buildings (Table 2-10). The results were used to generate CONUS maps for the fraction of injuries requiring hospitalization by EF number (Figure 2-17).

Table 2-10 Injury Type Fraction vs. EF Number and Building Type

Building type	EF#	Treat and release	Hospitalize
Manufactured (mobile homes)	0	0.89	0.11
	1	0.65	0.35
	2	0.35	0.65
	3	0.25	0.75
	4	0.25	0.75
	5	0.25	0.75
Others	0	1	0
	1	0.67	0.33
	2	0.65	0.35
	3	0.55	0.45
	4	0.43	0.57
	5	0.29	0.71

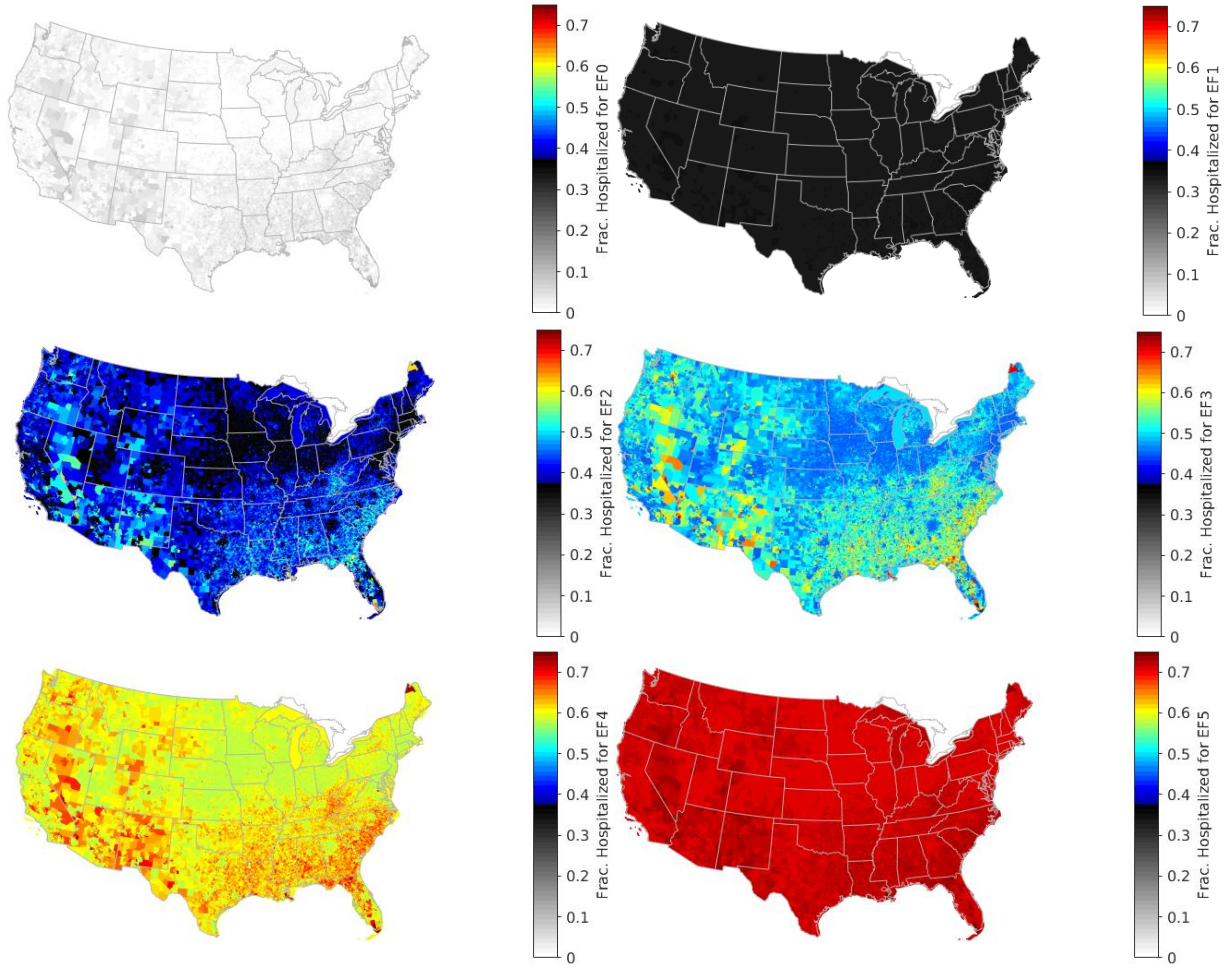

Figure 2-17. Modeled fraction of injuries that require hospitalization for (top left) EF0, (top right) EF1, (middle left) EF2, (middle right) EF3, (bottom left) EF4, and (bottom right) EF5 tornadoes.

2.3.6 Rapid Scan Benefits

Faster radar measurement updates could improve tornado warning lead time, POD, and FAR (Heinselman et al. 2015). However, weather radar volume update rate is constrained by the need to collect enough samples over the same space to reduce measurement error and improve clutter filtering, as well as by the limited agility of the antenna. WSR-88D volume coverage patterns (VCPs) designed for convective conditions have periods of 4.5 to 6 minutes, while TDWR hazard mode volume scans have ~2.5-minute periods (albeit with sparse sampling in elevation angle) and a 1-minute update time for base scans. In 2011,

the automated volume scan evaluation and termination (AVSET) algorithm was deployed on WSR-88Ds to adaptively shorten a VCP by skipping high-elevation cuts with no weather, and in 2014, the SAILS technique was introduced, giving operators the option to run an additional base scan during the middle of a VCP (Chrisman 2013). Subsequently, MESO-SAILS was added in 2016 to allow the insertion of multiple base scans within a VCP period (Chrisman 2014).

These new VCP algorithms allow better update rates in the elevation angles targeted for specific weather phenomena such as potentially tornadic storms. The scan rates are still ultimately limited by the radar resource. In the future, significantly faster updates could be enabled by operational deployment of electronically scanned phased array radars (e.g., Heinselman et al. 2008; Weber et al. 2017). Since we wish to apply our model to potential future radar networks, we need to quantify added benefits from rapid scanning.

We showed earlier that improvements in tornado warning POD and FAR can reduce casualty rates. Furthermore, previous studies have indicated that faster radar scanning can raise POD and lower FAR (Heinselman et al. 2015; Wilson et al. 2017). Therefore, combining the two dependencies, we were able to model the casualty-reduction benefits of rapid-scan radars.

The National Weather Radar Testbed (NWRT) (Heinselman and Torres 2011) was used in a series of phased array radar innovative sensing experiments (PARISE) to study the effects of faster scanning on weather forecasters making severe storm warning decisions. Tornadoes resulting from three storm types (squall line, supercell cluster, and supercell) were studied in the 2015 PARISE (Wilson et al. 2017), with surveillance volume update periods of 61–76 s. The radar data were sampled to generate full- (~1 minute), half- (~2 minutes), and quarter- (~5 minutes) speed outputs. Each temporal resolution set was given to a separate group of ten NWS forecasters for warning guidance. The quarter-speed case is representative of most of the weather radar data used in our regression analyses, so that can be considered the baseline condition.

The supercell case yielded no difference among the three groups, with a perfect score of POD = 1 and FAR = 0 across the board. The squall line case also showed little variation with update rate, with FAR = 1 for all groups, POD = 0.1 for the full- and half-speed groups, and POD = 0 for the quarter-speed group. The supercell cluster case generated the only notable response with POD increasing—0.1, 0.6, 0.8—and FAR decreasing—0.50, 0.53, 0.33—for the quarter-, half-, and full-speed groups.

Since these results were based on a very small sample size (thirty forecasters working on one null storm case and three storms that spawned five tornado events in total), we applied them conservatively. PARISE was conducted under fairly ideal radar coverage, so looking at Figure 2-9, we only considered changing the POD vs. FVO relationship close to FVO = 1. Since the maximum POD enhancement of 0.8 (at full scan rate) only exceeded the model values at FVO = 1 for the EF0–1 case, that was the only modeled relationship modified for the rapid-scan case. In other words, the POD performance of the EF2 and EF3–5 cases were already too good for a rapid-scan capability to add value. For one-minute update scans, we enhanced the POD vs. FVO relationship as indicated by the dashed line in the top left plot of Figure 2-9.

The new value of POD at FVO = 1 is given by $0.8u + (a + b)(1 - u)$, where a and b are taken from the EF0–1 high-FVO column in the bottom section of Table 2-2, and $u = 0.316$ is the fraction of CONUS tornadic storms that are of cluster type (Smith et al. 2012). This equation conservatively assumes that the POD enhancement due to rapid scanning is only effective on cluster storms.

Likewise, for FAR reduction, a similar logic was applied to arrive at the dashed line shown in Figure 2-12. The corresponding equation for one-minute scan FAR at CHR = 0 is $0.33u + a(1 - u)$, where a is taken from Table 2-4. The resulting changes to the curves in Figures 2-9 and 2-12 were applied in computing model results for rapid-scan scenarios.

Lengthening tornado warning lead times also lowers casualties, as we showed in section 2.3.4. Wilson et al. (2017) showed that the median lead time for tornado warnings increased in the squall line, supercell cluster, and supercell cases by 0, 7.5, and 3.5 minutes, respectively, for the full-speed groups relative to the quarter-speed groups. The fraction of CONUS tornadic storms of cluster type and discrete supercell type are 0.316 and 0.290 (Smith et al. 2012), so we computed an overall effective increase in median lead time as (7.5)(0.316) + (3.5)(0.290) = 3.385 minutes (203 s) for the rapid-scan case relative to baseline. This extra time was then added to the input lead time in the casualty model computation. To be conservative, this lead time enhancement was only directly applied to the EF0, EF1, and EF2 cases, since stronger tornadoes were not observed during the cited PARISE experiment. For the EF3–5 case, the rapid-scan improvement was restricted to match the EF2 case. Table 2-11 summarizes the median lead times used in the casualty estimation model. The baseline values were computed over all warnings with positive lead times in our 1998–2018 database. The EF3, EF4, and EF5 cases were combined because of the smaller number of cases.

Table 2-11 Median Tornado Warning Lead Times

EF#	0	1	2	3–5
Baseline (actual)	900 s	930 s	1020 s	1140 s
Rapid scan (modeled)	1103 s	1133 s	1223 s	1223 s

2.3.7 CONUS Grid Computation

We now combine the development presented in the previous sections to produce model estimates of the mean annual casualty cost due to tornadoes over the CONUS. The modeled tornado casualty rate (per year, per grid cell) is given by

$$R_{ijm}^{F,H,R} = \sum_{m=0}^{5} \left[r_{ijm}(1) B_{ijm} + r_{ijm}(0)\left(1 - B_{ijm}\right) \right] O_{ijm}\, Y_{ijm}^{F,H,R} , \qquad (2\text{-}5)$$

where B is the probability of warning per tornado, O is the tornado occurrence rate, i and j are the latitude and longitude grid indices, m is the EF number, and the superscripts denote fatal (F), injured—hospitalized (H), and injured—treated and released (R). The casualty type fractions are parsed as

$$Y_{ijm}^{F} = f_m \,, \tag{2-6}$$

$$Y_{ijm}^{H} = (1 - f_m)h_{ijm} \text{ , and} \tag{2-7}$$

$$Y_{ijm}^{R} = (1 - f_m)(1 - h_{ijm}) \,, \tag{2-8}$$

where f is the fatality fraction given by Table 2-8 and h is the fraction of injured that are hospitalized (Figure 2-17). From Equation 2-2, omitting the warning presence variable as discussed,

$$r_{ijm}(W) = \exp\left[\alpha \ln\left(D_{ij}A_{0m}\right) + \beta \ln S_m + \gamma M_{ij} + \delta F_{ij} + \zeta T_m(W) + k\right] \tag{2-9}$$

is the casualty rate per tornado with (W = 1) and without (W = 0) warning. $T_m(0) = 0$, and $T_m(1)$ is given by the entries in Table 2-11. F is the gridded FAR computed from our model via CHR and the relationship depicted in Figure 2-12. The regression coefficients used are given in Table 2-7. D is the population density. A_0 is the mean tornado path area and S is the mean tornado surface dissipation energy density (Table 2-8). The mean of the path area is taken in log space, since the distribution is closer to log-normal than to normal. To include as much data as possible, we went back to the beginning (1950) of the U.S. tornado database; however, data from 1950–1953 were excluded due to suspected quality issues (Ashley and Strader 2016). Tornadoes were sorted by EF number and accumulated in our 30-arcsec CONUS model grid. The sums were then smoothed with a 2D Gaussian kernel with a width of 0.5°, then divided by the number of years to get the annual tornado occurrence rate (Figure 2-18). Without any spatial smoothing, there would be too many grid cells with zero occurrence rate, which would not be realistic.

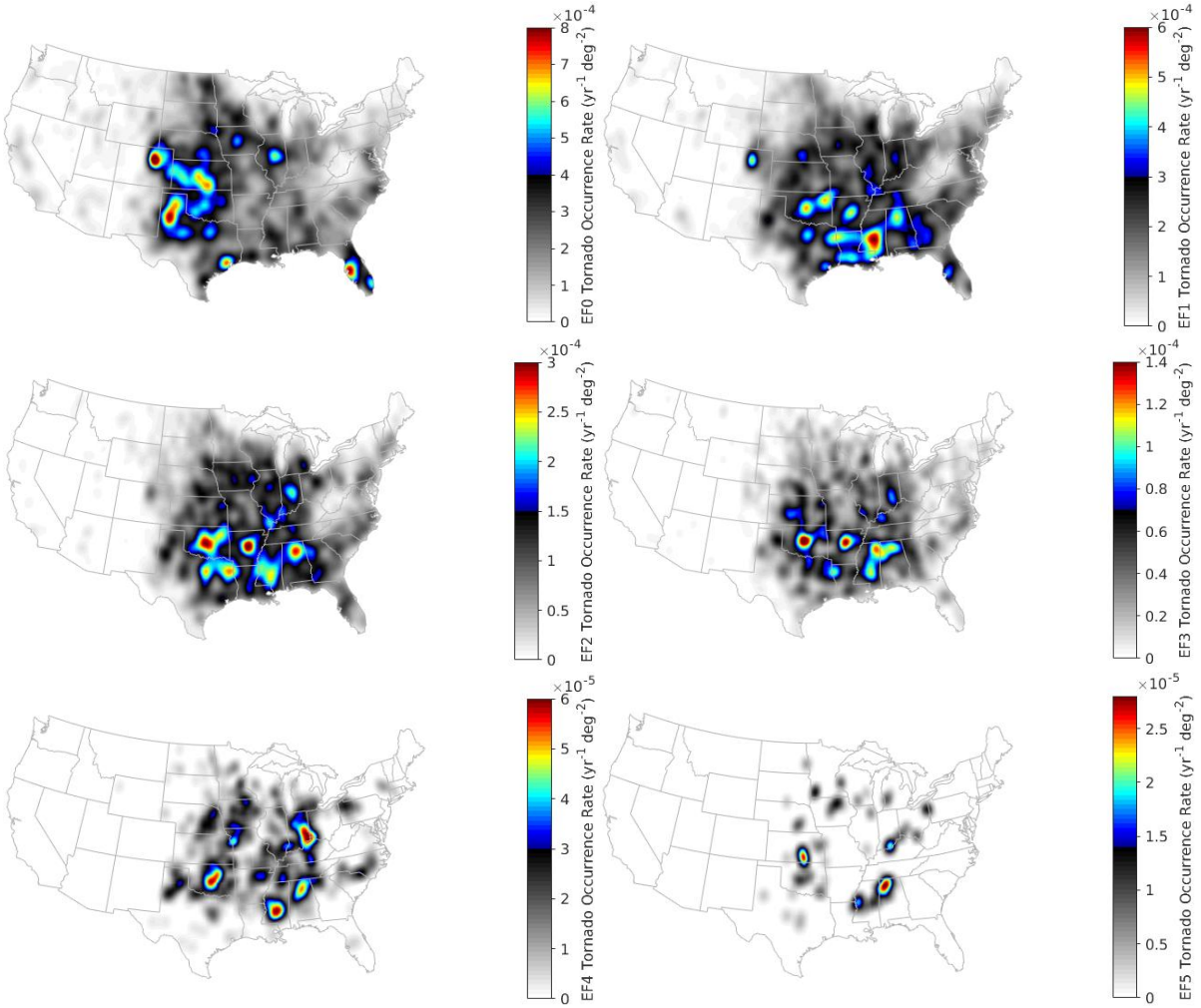

Figure 2-18. Historical (1954–2018) occurrence rate for (top left) EF0, (top right) EF1, (middle left) EF2, (middle right) EF3, (bottom left) EF4, and (bottom right) EF5 tornadoes. Note that a different color scaling was used for each map to enhance contrast.

The spatial features in the EF4 and EF5 cases of Figure 2-18 are likely not so robust due to the small number of tornadoes. The features in the lower EF cases, however, are probably meaningful. The three hot spots over central Oklahoma, Arkansas, and northern Alabama are notable, as they persist over the EF1, EF2, and EF3 cases. (The northern Alabama peak is also present for EF4 and EF5.) There may be an element of reporting bias at play, but this is, nonetheless, an interesting observation.

Summing Equation 2-5 across all grid indices and EF numbers yielded the predicted CONUS tornado casualty rate per year parsed by casualty type. The results were multiplied by the corresponding costs in Table 2-9 and summed to arrive at the total estimated annual CONUS tornado casualty costs.

2.3.8 Tornado Warning Sheltering Cost Reduction

As demonstrated, tornado warnings save lives. However, they can also exact a cost due to time spent sheltering by people who responded to the warnings. Strictly speaking, time spent sheltering when a tornado does not hit your building is time wasted. Since very few buildings are actually damaged by tornadoes, that adds up to a lot of lost time.

For a more nuanced take on this issue, we treat the cost of work and personal time losses separately. Work time lost is a loss regardless of whether a tornado warning was correct or a false alarm—the cost to society from loss of work time does not depend on the outcome of the warning. We posit, however, that personal time should only be considered a loss if the warning was a false alarm. That is, if one took shelter on a warning and a tornado touched down in the warning area, then one is likely to say that time spent sheltering was worthwhile from a personal perspective.

The mean per-person, per-hour cost of work-time lost while sheltering can be computed as

$$C_W = F_E F_W V_W \, , \tag{2-10}$$

where F_E is the fraction of the population that is employed, F_W is fraction of time spent working by those who are employed, and V_W is the mean wage per hour. This cost applies to sheltering on all warnings, true or false. The mean per-person, per-hour cost of personal time lost while sheltering only on a false alarm can be calculated as

$$C_P = F_E(1 - F_W)V_P + (1 - F_E)V_P \, , \tag{2-11}$$

where V_P is the value of personal time per unit time. We followed Sutter and Erickson (2010) in valuing personal time as 1/3 of the mean wage (V_W/3) after Cesario (1976). January 2019 total private sector employment numbers were taken from the U.S. BLS web site (https://www.bls.gov/ces/) to get F_E = 0.607, F_W = (34.5 h per week)/(168 h per week) = 0.205, V_W = \$27.56 h^{-1}, and V_P = (\$27.56 h^{-1})/3 = \$9.19 h^{-1}. Plugging these values into Equations 2-10 and 2-11, we get C_W = \$3.44 h^{-1} and C_P = \$8.04 h^{-1}.

The total annual added cost of sheltering due to tornado warnings is given by

$$C_S = HT\left(C_W \sum_{i,j}^{\text{CONUS}} I_{ij}\, P_{ij} + C_P \sum_{i,j}^{\text{CONUS}} I_{ij}\, P_{ij} F_{ij}\right), \tag{2-12}$$

where H is the shelter response rate, T is the mean time spent sheltering, I is the tornado warning issuance rate per year, P is population, and F is the modeled false alarm ratio for tornado warnings. Again, following Sutter and Erickson (2010), we assumed $H = 0.4$. We approximated the mean time spent sheltering by the mean tornado warning valid period computed over the storm-based warning era, which yielded $T = 0.574$ h. CONUS maps of I for the county-based and storm-based warning eras are shown in Figure 2-19. The CIESIN 2015 and 2020 gridded population data were interpolated to get current (2019) values.

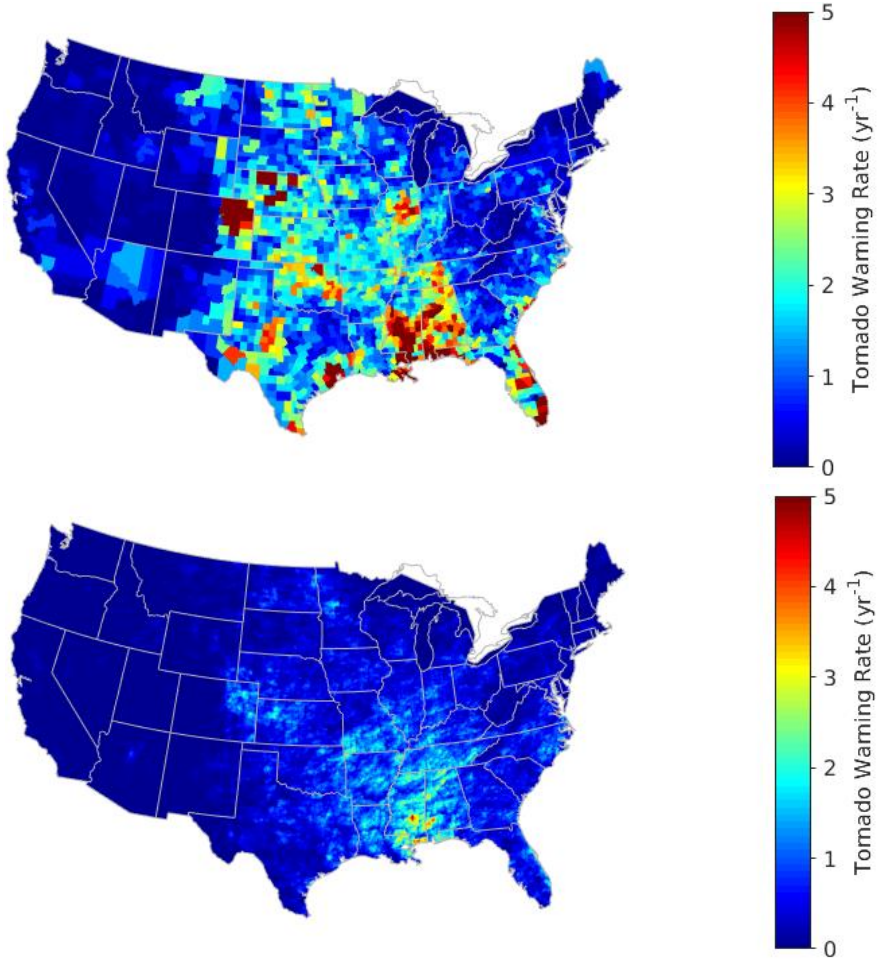

Figure 2-19. Mean annual tornado warning issuance rate over the (top) county-based (January 1998 to September 2007) and (bottom) storm-based warning (October 2007 to December 2018) eras within our study period.

2.3.8.1 Tornado Warning Sheltering Cost Reduction due to Storm-Based Warnings

As an aside, we can estimate the tornado warning sheltering cost savings associated with the switch from county-based to storm-based tornado warnings in 2007. Because the mean storm-based warning area is much smaller than the mean county-based warning area (Table 2-3), people at a given location experience fewer warnings per year, which is apparent in Figure 2-19. The decrease of I in Equation 2-12 results in lower cost. The mean FAR is also slightly lower in the storm-based warning period (Table 2-3). Using 2019 population, employment, and dollar values, we get total sheltering costs of $1027M per year with county-

based warnings and $295M per year with storm-based warnings. That is a savings of $732M per year in 2019 dollars.

2.4 MODEL SUMMARY

To recap briefly, we developed a geospatial model for calculating weather radar benefits for tornadoes. We showed that certain radar performance and coverage metrics impacted tornado warning statistics (detection probability and false alarm ratio), which, in turn, affected casualty rate and loss of work and personal time in sheltering (Figure 2-20). The model operates on a high-resolution spatial grid over the CONUS capable of revealing regional variances. It can take as input any hypothetical radar network configuration.

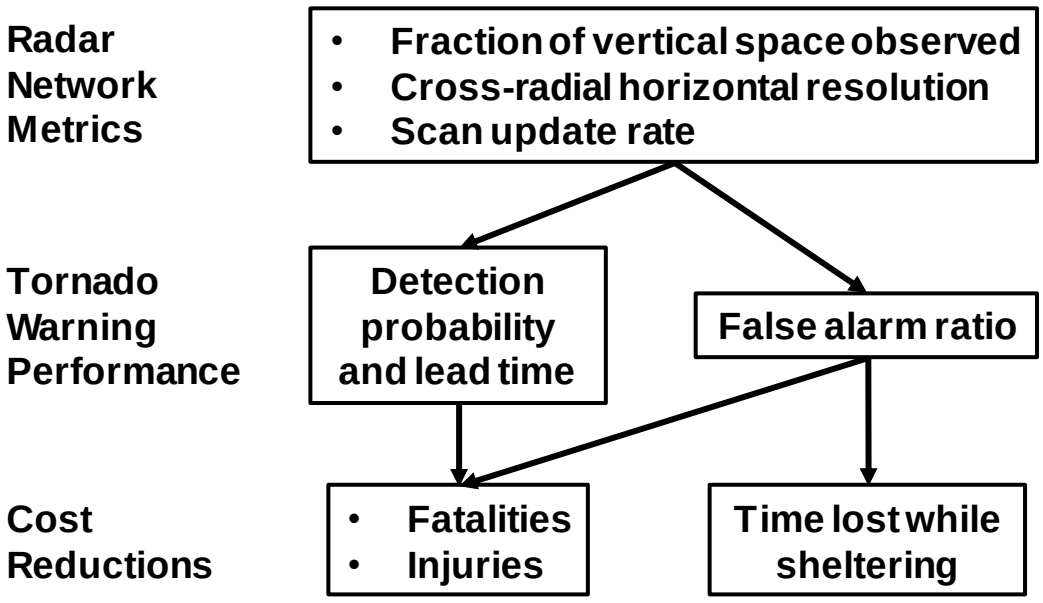

Figure 2-20. Simplified flow chart of weather radar tornado benefits model.

The "fraction of vertical volume observed" measure of radar network coverage is new to tornado warning performance analysis. It takes into account the near-range cone of silence, the far-range loss of low-level coverage due to the Earth's curvature, as well as terrain blockage and ground height variability. It was instrumental in establishing an unambiguously positive correlation between radar coverage and tornado warning performance.

Although our model treats the detection probability and false alarm ratio separately and independently, in reality these two statistical measures are intertwined. Ideally, we want detection probability to approach

1, while eliminating false alarms altogether. In general, this is not realistic; increasing detection probability tends to also increase FAR. To take this dependence into account, various statistical measures have been devised, such as the area under the receiver operating curve (AUC) and critical success index (CSI), to provide a single metric for optimization. This type of approach is also advocated for quantifying tornado warning performance (Brooks and Correia 2018). However, we were not able to employ an integrated warning performance metric in our model for the following reasons. (1) The casualty regression analysis was best done on an event-by-event basis, where the key statistic is the presence/absence of warning; this precluded use of an averaged statistical measure of detection. (2) Even if we wanted to apply an integrated statistical warning performance measure in the casualty regression, the detection probability is so heavily dependent on EF number that parsing by EF value would need to be done. False alarms, on the other hand, cannot be parsed by EF number, so that made use of an integrated metric impossible.

An earlier version of our tornado benefit model was presented in a refereed publication (Cho and Kurdzo 2019a). The changes made to the model since that time are as follows.

1. The final year of the tornado and warning data used for analysis and model input was updated from 2017 to 2018.
2. VSL, employment data, and population estimates were updated from 2018 to 2019.
3. The warning presence variable was dropped in lieu of a lead time variable in the casualty regression model.
4. Rapid scanning impact on warning lead time was added.
5. Work time lost during sheltering on true tornado warnings was added to the sheltering cost model.
6. The tornado occurrence rate map smoothing operation was modified. Previously, the historical occurrences were accumulated in a coarse CONUS grid, then mapped to the finer model grid via 2D linear interpolation. Now, the accumulation is done directly on the model grid, then smoothed using a 2D Gaussian kernel.
7. An error was corrected in the tornado path to FAR map grid points matching code, which improved the casualty regression model statistics for the historical mean FAR predictor variable.

In the next chapter, we use our model to compute monetized tornado-related benefits for various CONUS weather radar network configurations.

This page intentionally left blank.

3. BENEFIT CALCULATIONS

3.1 BASIC SCENARIOS

Before considering a variety of hypothetical CONUS weather radar networks, we computed modeled tornado casualty and false alarm costs for six basic radar network configurations: (1) No radar coverage, (2) WSR-88Ds, (3) WSR-88Ds and TDWRs (current baseline), (4) WSR-88Ds and TDWRs with rapid scanning, (5) perfect radar coverage with current scanning capability, and (6) perfect radar coverage with rapid scanning. The no radar coverage case was simulated by setting FVO = 0 and CHR = ∞ everywhere. Comparison with the no-radar case allows an estimate of the benefit added by any radars, while comparison with the baseline yields benefits above what we currently have. Comparison of the WSR-88D-only case with the baseline yields the incremental benefit of TDWRs for tornadoes. The perfect coverage cases were handled by setting FVO = 1 and CHR = 0 everywhere; these configurations allow estimates of the remaining benefit pools over the baseline. Rapid scanning assumes a one-minute volume update rate.

Table 3-1 gives the tornado casualty estimates for the six basic scenarios, as well as the actual mean annual casualty rates. There is excellent agreement between the baseline model results and the actual mean casualty rates—they are well within the actual annual standard deviation variabilities. Table 3-2 lists the corresponding tornado casualty costs, and Table 3-3 adds the estimated costs due to time spent sheltering under warning. All costs are in 2019 dollars.

Table 3-1 Annual CONUS Tornado Casualty Estimates for Basic Scenarios

Scenario	Fatal	Injured (hospitalized)	Injured (treated and released)	Total	Delta baseline
No radar coverage	102	678	573	1353	195
WSR-88D	88	583	493	1164	6
WSR-88D, TDWR	87	580	491	1158	——
WSR-88D, TDWR, rapid scan	78	521	440	1039	-119
Perfect coverage	82	547	463	1092	-66
Perfect coverage, rapid scan	69	459	388	916	-242
Actual mean (1998–2018)	78 ± 25	1060 ± 248[a]		1138 ± 273	N/A

[a]Actual average injured counts are totals, not broken out by injury type.

Table 3-2 Annual CONUS Tornado Casualty Cost Estimates for Basic Scenarios

Scenario	Fatal ($M)	Injured (hospitalized) ($M)	Injured (treated and released) ($M)	Total ($M)	Delta baseline ($M)
No radar coverage	1184	2092	313	3589	519
WSR-88D	1017	1798	269	3084	14
WSR-88D, TDWR	1012	1790	268	3070	——
WSR-88D, TDWR, rapid scan	909	1608	240	2757	-313
Perfect coverage	955	1687	252	2894	-176
Perfect coverage, rapid scan	802	1416	211	2429	-641

Table 3-3 Annual CONUS Tornado Casualty and Sheltering Cost Estimates for Basic Scenarios

Scenario	Casualty ($M)	Sheltering ($M)	Total ($M)	Delta baseline ($M)
No radar coverage	3589	315	3904	535
WSR-88D	3084	301	3385	16
WSR-88D, TDWR	3070	299	3369	——
WSR-88D, TDWR, rapid scan	2757	279	3036	-333
Perfect coverage	2894	292	3186	-183
Perfect coverage, rapid scan	2429	264	2693	-676

Casualty and cost differences from the current baseline are listed in the "Delta baseline" columns of Tables 3-1 to 3-3. Relative to a CONUS without weather radars, the current baseline provides over half a billion dollars in tornado benefits annually. The perfect coverage, rapid scan case shows that the remaining benefit pool is somewhat larger. The incremental benefit of TDWRs is modest at $16M per year, which is not surprising since they mostly cover the same areas as the WSR-88Ds. Adding rapid scanning capability achieves far greater cost reduction than improving radar coverage—just upgrading the existing radars with rapid scanning yields about 80% more benefit as blanketing the CONUS with perfect radar coverage.

There is a caveat with the rapid scanning results. Since there are no operational weather radars conducting volume scans at a rate of one per minute, our rapid scan FAR reduction model was necessarily

based on a limited number of experiments carried out with the NWRT phased array radar. Other parts of our cost model were based on large numbers of tornadoes and warnings (Tables 2-1 and 2-3), inspiring a much higher degree of confidence. Since the overall results indicated high benefit leverage through rapid scanning, it would be prudent to gather more statistics on the effects of faster volume scans on tornado warning performance by utilizing existing and new radars capable of fine temporal resolution observations (e.g., Stailey and Hondl 2016; Kurdzo et al. 2017). With the recent implantation of SAILS and MESO-SAILS (faster surface scan updates), there may soon be enough data to analyze potential tornado warning performance improvement due to these scan modes.

Figure 2-18 indicates that most of the CONUS tornado activity exists east of the Rockies. This suggests that perhaps most of the tornado-related benefits also exists in the east. To show this explicitly, we computed the annual tornado casualty and sheltering cost estimates for the CONUS east of 106° W longitude (Table 3-4). The "Delta baseline" column is almost identical to the one in Table 3-3. So as far as tornadoes are concerned, radars in the West have almost no leverage in generating benefits.

Table 3-4 Annual CONUS Tornado Casualty and Sheltering Cost Estimates for Basic Scenarios East of the Rockies

Scenario	Casualty ($M)	Sheltering ($M)	Total ($M)	Delta baseline ($M)
No radar coverage	3583	311	3894	533
WSR-88D	3080	297	3377	16
WSR-88D, TDWR	3066	295	3361	——
WSR-88D, TDWR, rapid scan	2753	275	3028	-333
Perfect coverage	2890	288	3178	-183
Perfect coverage, rapid scan	2426	260	2686	-675

3.1.1 Tornado warning benefit

As an aside, we could ask what the current tornado warning cost/benefit balance is between casualty reduction benefit vs. the total cost due to sheltering. In other words, do present-day tornado warnings provide a net positive benefit as monetized by our model? This is different from asking how much benefit radars provide through tornado warning performance improvement.

In order to answer this question, we need to simplify the casualty regression model to exclude FAR effects (since false alarms are meaningless in a world without alarms), and include presence of warning instead of lead time. In other words, we omit the F_0 and T terms from Equation 2-2. The resulting regression coefficient estimates are given in Table 3-5, and the corresponding casualty and cost estimates for the no-warning cases are given in Table 3-6.

Table 3-5 Tornado Casualty Model Regression Results without FAR and Lead Time Variables

Coefficient	Estimate	Std. error	z	Pr (> |z|)
α (log. population)	0.313	0.0121	25.9	$< 2 \times 10^{-16}$
β (log. energy density)	5.98	0.127	46.9	$< 2 \times 10^{-16}$
γ (mobile home fraction)	1.76	0.195	9.01	$< 2 \times 10^{-16}$
ε (warning presence)	-0.740	0.0656	-11.3	$< 2 \times 10^{-16}$
k (intercept constant)	-66.7	1.36	-48.9	$< 2 \times 10^{-16}$
θ (dispersion parameter)	0.139	0.00455	N/A	N/A

Table 3-6 Annual CONUS Tornado Casualty and Cost Estimates for No Tornado Warnings

Parameter	Fatal	Injured (hospitalized)	Injured (treated and released)	Total
Casualty	151	1000	833	1983
Cost ($M)	1746	3085	454	5286

Subtracting the estimated current annual casualty cost of $3070M (Table 3-3) from the estimated cost for the no-warning scenario in Table 3-6 ($5286M) yields $2216M—this is the estimated annual CONUS benefit of having tornado warnings (with current performance statistics). Since the current total cost of sheltering on tornado warnings is $295M per year (section 2.3.8.1), the answer is yes, there is a net benefit for tornado warnings of $1921M per year.

3.2 RADAR NETWORK UPGRADE SCENARIOS

Aside from the WSR-88D and TDWR, which are weather-specialty radars, there are primary air surveillance radars in the U.S. that provide some degree of weather observation capability as well. These are the FAA's Airport Surveillance Radars (ASRs), including those with a Weather Systems Processor (WSP) (Cho et al. 2015), and their military equivalents (Ground Position Navigation (GPN) radars), Air Route Surveillance Radar-4 (ARSR-4), and the Common Air Route Surveillance Radar (CARSR). Figure 3-1 shows a map of their locations. Within the CONUS there are 294 ASR/GPNs (33 with WSPs), 40 ARSR-4s, and 73 CARSRs, excluding training and support systems. It is possible that one or more of these radar types could be replaced by future systems with upgraded weather observation capability. Of course,

requiring higher quality weather data from new radars would increase their cost. Thus, it is of interest to quantify the additional benefits such a move would yield.

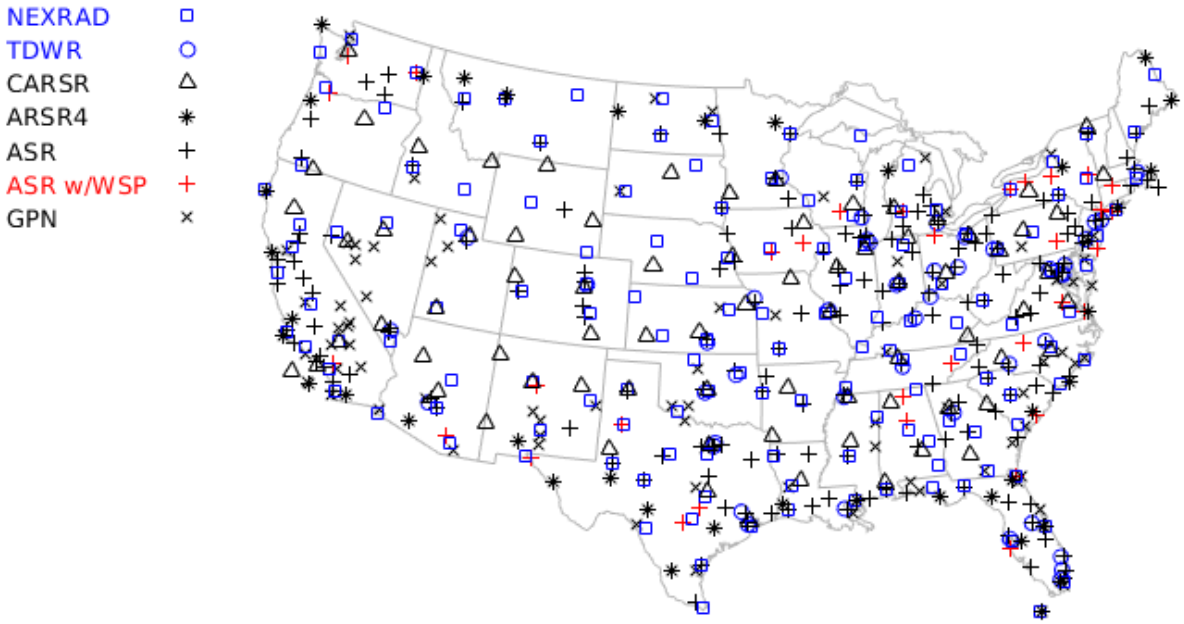

Figure 3-1. Locations of NEXRAD, TDWR, and primary air surveillance radars with weather observation capability.

3.2.1 One-to-one radar replacement

The existing radar networks could be upgraded separately without any attempt to consolidate coverage and sites using new multi-mission radars. In this case, the systems would likely be replaced one-to-one at every site. We considered various potential permutations of upgrades to these networks.

In order to compute the coverage and spatial resolution of the hypothetical network upgrades, we needed to assign some basic parameters for the new radars. For the ASR/GPN replacement, we assumed a 2° azimuth resolution and maximum elevation angle of 60°, with the same coverage range (110 km) as the current systems. For the long-range radar (ARSR-4 and CARSR) replacement, we assumed a 1.7° azimuth resolution and maximum elevation angle of 30°, with the same coverage range (460 km) as the current systems. We also considered cases with (~1 minute update) and without (~5 minute update) rapid scanning. These parameters are consistent with early SENSR performance requirements. (Since then, SENSR has been de-scoped to exclude weather missions except for the ARSR-4 replacement sites.)

Because there were a large number of permutations possible, we ran a limited number of combinations for added weather capability at the following sets of locations: (1) ASR/GPN sites, (2) ARSR-4 sites, (3) ASR/GPN and ARSR-4 sites, (4) ARSR-4 and CARSR sites, (5) ASR/GPN, ARSR-4, and CARSR sites, and (6) ASR-9 WSP sites. The addition of weather capability at CARSR sites without a corresponding upgrade at ARSR-4 sites is unlikely, due to the overlap with the WSR-88D network, so we did not include those cases. The rapid scan option was not applied to individual radar types, but to the legacy weather radars (WSR-88D and TDWR) as a group and to the hypothetical aircraft surveillance radar replacements as a group, which also cut down on the number of potential network configurations.

Results for these scenarios are given in Table 3-7. To keep the table size manageable, casualty counts and injury type breakdowns are not provided. For brevity, the following codes are used for the scenario cases: N = NEXRAD (WSR-88D), T = TDWR, A = ASR/GPN replacement, 4 = ARSR-4 replacement, C = CARSR replacement, and W = ASR-9 WSP replacement. Subscript "R" is used to denote rapid scan capability. Presence of a particular radar type in a given scenario means that all the current CONUS sites for that type would be populated with a radar with quality weather output capability.

Table 3-7 Annual CONUS Tornado Cost Estimates for Augmented Network Scenarios

Scenario	Casualty ($M)	Sheltering ($M)	Total ($M)	Delta baseline ($M)	Delta baseline per upgraded site ($k)
N, T (baseline)	3070	299	3369	——	——
N_R, T_R	2757	279	3036	-333	-1781
N, T, A	3050	298	3348	-21	-71
N, T, A_R	2999	292	3291	-78	-265
N_R, T_R, A	2757	279	3036	-333	-692
N_R, T_R, A_R	2724	276	3000	-369	-767
N, T, 4	3069	299	3368	-1	-25
N, T, 4_R	3067	299	3366	-3	-75
N_R, T_R, 4	2757	279	3036	-333	-1467
N_R, T_R, 4_R	2756	279	3035	-334	-1471
N, T, 4, C	3061	299	3360	-9	-80
N, T, 4_R, C_R	3039	298	3337	-32	-283
N_R, T_R, 4, C	2757	279	3036	-333	-1110
N_R, T_R, 4_R, C_R	2742	279	3021	-348	-1160

N, T, A, 4	3050	298	3348	-21	-63
N, T, A_R, 4_R	2996	292	3288	-81	-243
N_R, T_R, A, 4	2757	279	3036	-333	-639
N_R, T_R, A_R, 4_R	2723	276	2999	-370	-710
N, T, A, 4, C	3044	298	3342	-27	-66
N, T, A_R, 4_R, C_R	2974	292	3266	-103	-253
N_R, T_R, A, 4, C	2757	279	3167	-333	-561
N_R, T_R, A_R, 4_R, C_R	2713	276	2989	-380	-640
N, T, W	3066	299	3365	-4	-121
N, T, W_R	3041	297	3338	-31	-939
N_R, T_R, W	2757	279	3036	-333	-1514
N_R, T_R, W_R	2751	278	3029	-340	-1546

From Table 3-7, we see that the most per-site benefit is obtained by upgrading the WSR-88Ds with rapid scan capability. With respect to upgrades to other radar networks, the WSP locations provide the most benefit per site. This can be explained by the fact that these sites tend to be near medium to large cities with significant convective weather potential, and are mutually exclusive with TDWR locations. Overall, without rapid scan capability, the addition of high-quality weather observation at non-baseline sites does not add much value with respect to tornado cost reduction.

3.2.2 Replacement with MPAR

For over a decade, FAA and NOAA have been studying the feasibility of replacing their single-mission radars with scalable multifunction phased array radars (MPARs) (Weber et al. 2007; Zrnic et al. 2007). Because of the coverage overlap provided by the current single-mission radar networks, a unified MPAR replacement plan could decrease the total number of radars needed to cover the same airspace, which might lead to lower acquisition and sustainment costs. While the scenarios of the previous section assumed one-to-one replacement of the current radars, an MPAR-type solution can lead to site consolidation. Therefore, in this section we examine MPAR-based scenarios, leveraging a previous siting analysis that was conducted for the FAA (Cho 2015).

Here we consider three of the radar replacement scenarios presented in the MPAR siting analysis: (I) Terminal radars replaced by MPAR, (II) WSR-88D and terminal radars replaced by MPAR, and (III) WSR-88D, terminal radars, and LRRs replaced by MPAR. As a fourth scenario (IV), we add a case where the WSR-88D and LRRs are replaced by MPAR, using the same methodology as Cho (2015). In this section, “terminal radars” are ASRs, GPNs, and TDWRs; LRRs are CARSRs and ARSR-4s.

In the siting study, two MPAR sizes were assumed for more cost-efficient coverage of the heterogeneous (terminal, en route, off-shore) air space—a full-size MPAR and a scaled down terminal MPAR (TMPAR). Table 3-8 lists their assumed characteristics. Each radar was assumed to have fixed planar phased array faces—four for full azimuthal coverage, and one to three where only selective azimuthal coverage was deemed necessary. Only existing radar sites (Figure 3-1) were considered for MPAR placement, i.e., no "green field" sites were allowed. See Cho (2015) for more details about the siting methodology.

Table 3-8 Assumed MPAR Characteristics

Parameter	MPAR	TMPAR
Range resolution (weather)	0.15 km	0.15 km
Maximum elevation angle	60°	60°
Elevation angle resolution (weather)[a]	1°	2°
Azimuthal resolution (weather)[a]	1°	2°
Minimum detectable weather reflectivity at 20 km[b]	-19 dBZ	-1 dBZ

[a]These are approximate values. They would actually vary with scan angle.
[b]These values are for horizon scans. They would be degraded with increasing elevation angle due to deliberate transmit beam widening that speeds up volume scan rates.

For the CONUS, the reductions in system count for MPAR compared to the legacy radar networks are shown in Table 3-9. Overall, similar or better air space coverage is provided by the MPAR networks with fewer sites, although not necessarily in specific locations, especially at low altitude. The MPAR site map for each scenario is given in Figure 3-2.

Table 3-9 Reduction in Number of Radars

Scenario	Legacy	MPAR + TMPAR	Change	% Reduction
I	339	42 + 249 = 291	-48	14%
II	482	160 + 180 = 340	-142	29%
III	598	197 + 187 = 384	-214	36%
IV	259	171 + 0 = 171	-90	34%

The specific MPAR locations for our scenarios I, II, and III are given in Appendix A of Cho (2015), where they are called scenarios 1G, 2G, and 3G, respectively. Since scenario IV is new, we provide the MPAR locations in Appendix A at the end of this report.

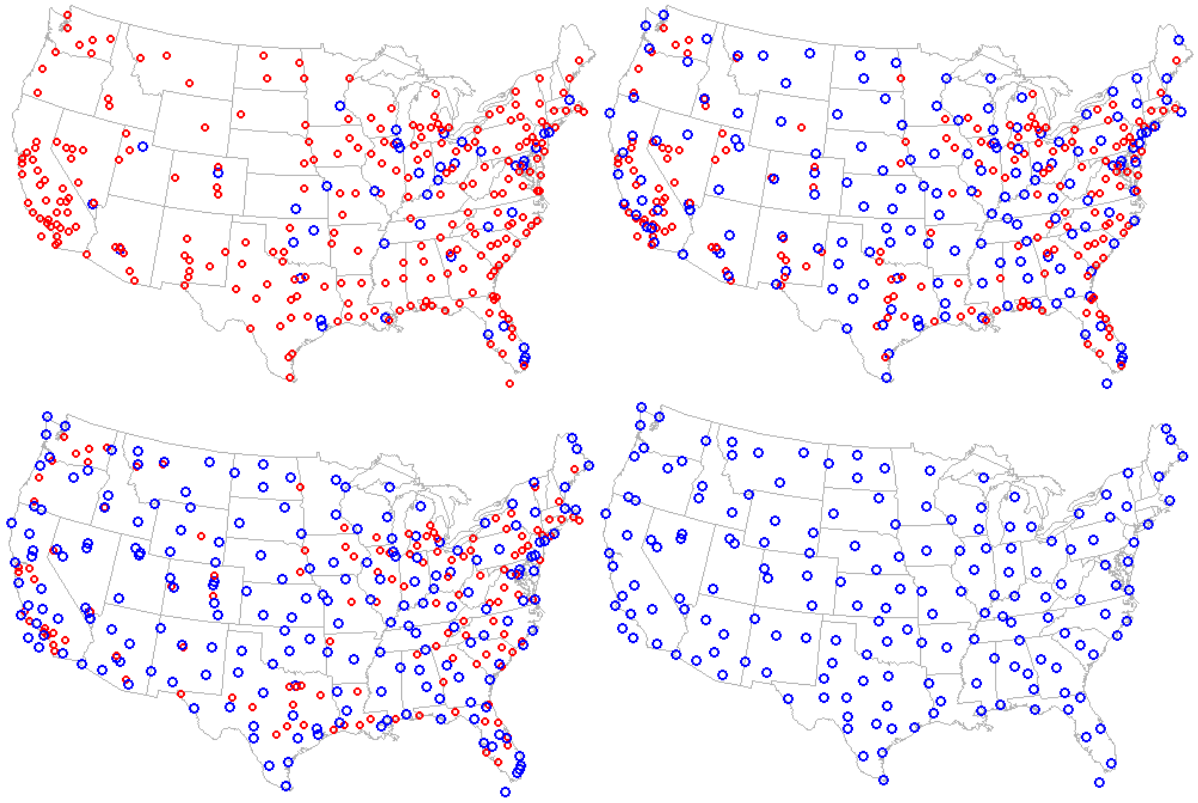

Figure 3-2. MPAR locations for scenarios (top left) I, (top right) II, (bottom left) III, and (bottom right) IV. Blue is MPAR, red is TMPAR.

From a purely coverage efficiency perspective, replacing WSR-88Ds and LRRs with MPARs (scenario IV) makes the most sense, because there is tremendous overlap between their coverages. The terminal surveillance missions, on the other hand, do not allow much reduction in radar count, aside from the elimination of TDWR sites. The low-altitude coverage around each airport must be maintained, so a TMPAR or MPAR is located at virtually all the existing ASR/GPN sites. This contrast can be seen in the Figure 3-2 maps, with scenario IV having much more evenly spaced sites than the other cases that include replacement of terminal radars.

Table 3-10 gives the annual CONUS tornado cost estimates and the benefits relative to baseline for the MPAR scenarios. Scenario I has two subcases—with and without an upgrade of the WSR-88D for rapid-scan capability. We assume that MPAR and TMPAR have rapid-scan capability. Scenario I without a WSR-88D upgrade is nearly equivalent to the N, T, A_R scenario of Table 3-7. Scenario IV provides the most benefit per upgraded site (nearly \$2M yr^{-1} per site) of all the scenarios examined, as might be expected given the massive coverage redundancy of the replaced legacy networks.

Table 3-10 Annual CONUS Tornado Cost Estimates for MPAR Scenarios

Scenario	Casualty ($M)	Sheltering ($M)	Total ($M)	Delta baseline ($M)	Delta baseline per upgraded site ($k)
N, T (baseline)	3070	299	3369	——	——
I	2998	292	3290	-79	-271
I (rapid scan WSR-88D)	2723	276	2999	-370	-853
II	2738	277	3015	-354	-1041
III	2735	276	3011	-358	-932
IV	2759	280	3039	-330	-1930

A more targeted set of additional sites could yield increased "bang for the buck." In the next section, we provide an example of such a gap filling exercise.

3.3 GAP FILLING EXAMPLE

Maps of cost density could also be used to analyze optimal locations for radars (e.g., Kurdzo and Palmer 2012). Figure 3-3 shows the tornado cost density map for a world without weather radars. If helping generate tornado warnings were the sole mission of weather radars, then this map could be used to optimize radar locations. Obviously, that is not the case, but if similar cost density maps could be developed for other major weather radar objectives such as flash flood cost reduction (Cho and Kurdzo 2019b; Kurdzo et al. 2019), then they could be combined to form the basis for a "clean slate" siting study.

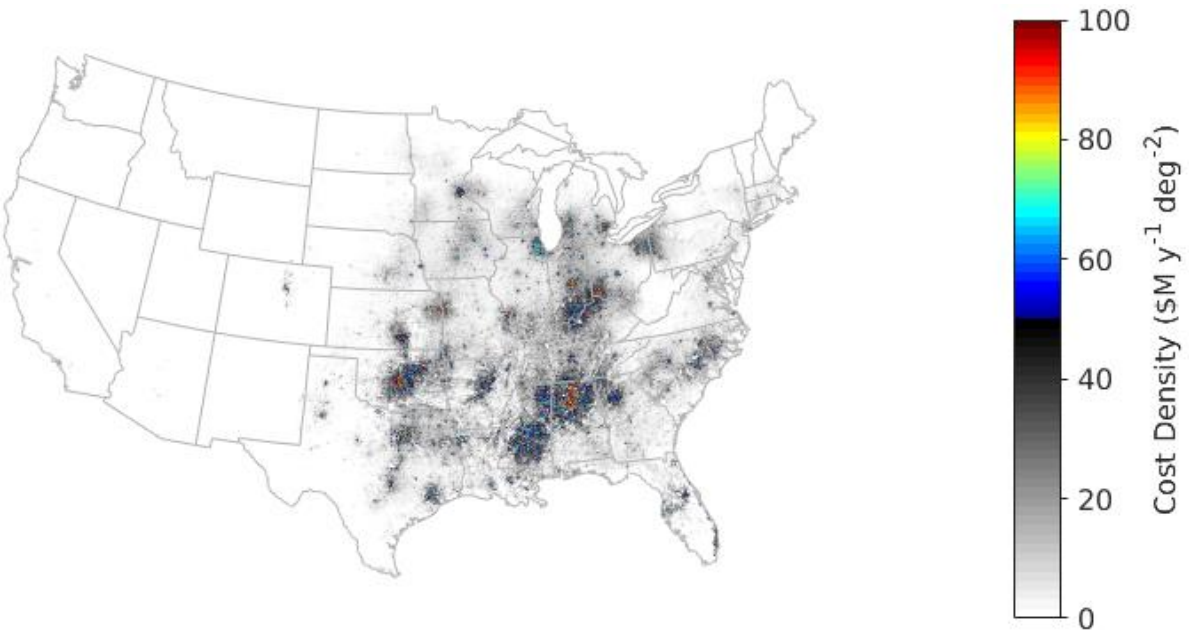

Figure 3-3. Tornado cost density map for the no-radar case.

Here we provide an example of a gap-filling exercise based only on tornado benefits. The left-hand plot of Figure 3-4 shows the cost density difference between the current baseline and perfect coverage (without rapid scanning), which shows the areas with the largest remaining benefit pools. Although the small-scale details are dominated by the high dynamic range of the population density, and much of the larger-scale modulation is due to high-EF tornado occurrence rate, the radar coverage deficiencies are also visible, e.g., the honeycomb-like pattern in the Midwest. The prevalence of mobile housing is also a factor, as Strader and Ashley (2018) highlighted in pointing out the higher tornado vulnerability of Alabama relative to Kansas.

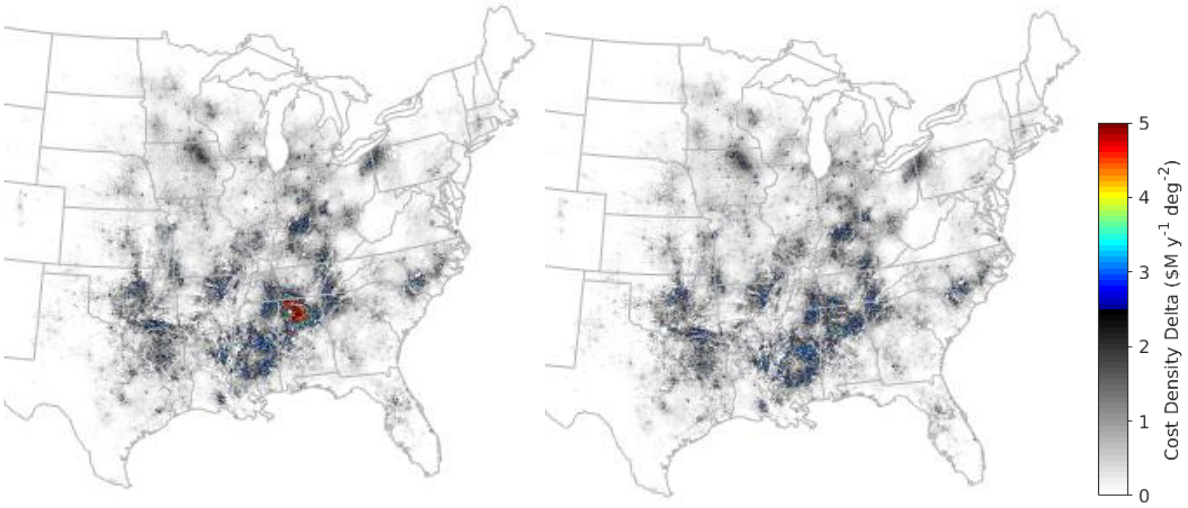

Figure 3-4. Tornado casualty and false alarm sheltering cost density difference, where the reference density is the perfect radar coverage case (without rapid scanning), for (left) the baseline network and (right) the baseline network with a WSR-88D added at Cullman Regional Airport in Alabama.

The cost density difference map shows a particularly strong peak in northern Alabama that manifests as a dark red patch. In order to fill this deficiency, we selected a site in the middle of the patch—Cullman Regional Airport (Figure 3-5)—at which to place a hypothetical WSR-88D in Cullman, Alabama ("KCMD"). Cullman lies right between two population centers and WSR-88Ds in Birmingham and Huntsville. The right-hand plot in Figure 3-4 shows the resulting cost density difference, indicating that the gap has been filled in effectively. The subsequent tornado casualty and sheltering cost reduction is $4M per year. If the WSR-88Ds and TDWRs are upgraded with rapid scan capability, the additional benefit provided by a rapid-scan WSR-88D at Cullman is $7M per year. These seem like fairly modest gap-filling benefits, but they are significantly more than the per-site benefits provided by the non-targeted network augmentation scenarios of Tables 3-7 and 3-10. Considering other unaccounted-for benefits (e.g., QPE improvement) and the decades-long lifetimes of radars, there may be a business case to be made for such a gap filler.

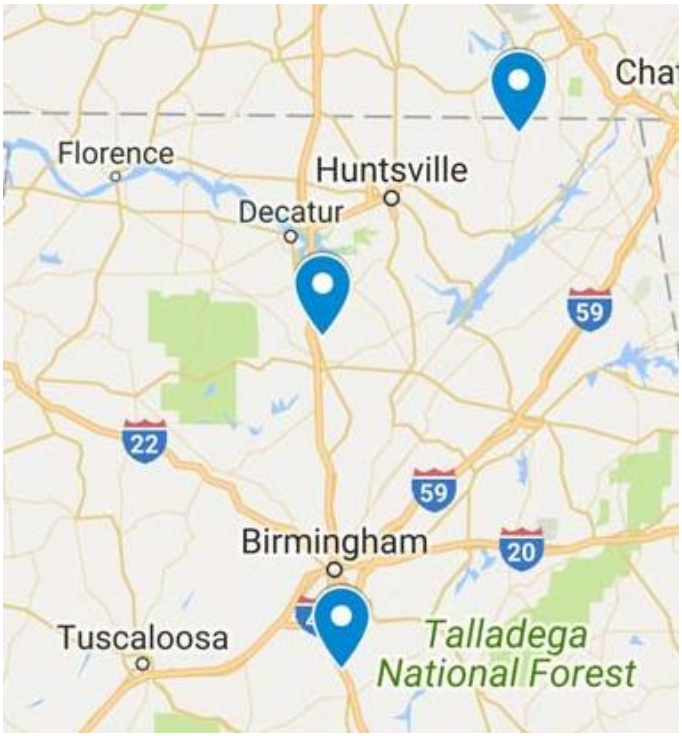

Figure 3-5. Locations of (center marker) Cullman Regional Airport, (top marker) KHTX WSR-88D, and (bottom marker) KBMX WSR-88D (courtesy of Google Maps).

The gap filling analysis could potentially be automated by using the cost density metric within an optimization scheme. Given a finite set of potential radar sites, the most beneficial top N additions could be determined through global optimization and/or exhaustive search.

This page intentionally left blank.

4. SUMMARY DISCUSSION

Through historical geospatial analyses, we were able to establish and quantify relationships between weather radar network coverage and tornado warning performance. Specifically, improvements in fraction of vertical volume observed and cross-radial horizontal resolution were linked to better tornado detection probability and false alarm rates, while faster radar scan updates were associated with enhanced POD, FAR, and longer warning lead times. Better tornado warning performance (POD and lead time) and lower historical FAR in a particular location were, in turn, linked to casualty rate reduction. Combining these relationships led to a geospatial model for estimating tornado casualty rates based on a given meteorological radar network. Monetizing casualties (fatalities and two injury classes) based on a standard value-of-statistical-life method yielded casualty costs. The value of time (work and personal) lost due to sheltering, which is dependent on FAR, was added to complete the tornado cost model. The difference in cost relative to a baseline yielded the monetized benefit.

Our model showed that the current weather radar network provides $535M per year benefit with respect to CONUS tornado cost reduction. 97% of this benefit is attributed to casualty reduction, and the rest to sheltering cost reduction. 99.6% of the benefit is realized east of the Rockies, due to the very geographically inhomogeneous tornado occurrence distribution.

There is a remaining benefit pool of at least $676M per year. The majority of this pool is due to faster scanning (one-minute volume update) radars. Since perfect radar coverage over the CONUS (or anything close to it) would be extremely expensive, upgrading existing sites with faster-scanning radars may be a more cost-effective way to harvest more of those benefits (for tornadoes). Note, however, that the quantification of rapid scan effects was based on a small number of experiments and is less robust than the other parts of our benefit model. In order to drive down this uncertainty, we recommend gathering more statistics on the effects of faster volume scans on tornado warning performance by utilizing existing and new radars capable of fine temporal resolution observations (e.g., Stailey and Hondl 2016; Kurdzo et al. 2017).

Targeted gap filling at benefit-heavy locations like northern Alabama may also be warranted. Gap locations, however, are dependent on the historical occurrence rate of high-EF-number tornadoes, of which the sample size is small, i.e., the uncertainty of this quantity is fairly high. Furthermore, areas of high tornado occurrence has been slowly shifting eastward, which may be related to the movement of the dry line due to climate change (Gensini and Brooks 2018). This migration may lead to even stronger cost-density gaps in the eastern U.S., where population density is generally higher and there is a greater concentration of mobile housing.

Tornado warning FAR is positively correlated with casualty rate and incurs added cost due to work and personal time lost during sheltering. The current FAR is high (0.72) relative to other severe weather warnings. For example, in the mid-2000s, NWS warning FARs were 0.46 for flash floods, 0.31 for winter storms, 0.31 for high winds, and 0.48 for severe thunderstorms (Barnes et al. 2007). This has not escaped the notice of mass media (Stirling 2015). There has been a slow decrease in FAR in recent years, due to an

apparent increased focus on this issue (Brooks and Correia 2018), but there is still room for improvement (although POD should not be sacrificed for this purpose). Reducing the current FAR of 0.72 is a worthy goal that taps into the sheltering cost reduction benefit. Making progress in this direction, however, is complicated and involves much more than improving weather radar data.

As discussed earlier, tornadoes are just one type of hazardous weather to consider when planning a weather radar network. Flash flooding is another deadly phenomenon for which we have developed an analogous benefit model (Cho and Kurdzo 2019b). Other uses of meteorological radar data, such as assimilation by numerical weather forecast models, also should be assigned monetized values. Extensive analyses will be required to form a comprehensive benefit case for future weather radar solutions.

APPENDIX A: SITE-BY-SITE LISTING OF SCENARIO IV MPAR LOCATIONS

The scenario IV MPAR CONUS locations are listed below, grouped by legacy radar type. If fewer than four antenna faces are specified, this is indicated by the number of faces and azimuth coverage range in parentheses.

Table A-1 ARSR-4 Sites

Site ID	Site Name	State	Replacement Radar
AJO	AJO	AZ	MPAR
CTY	CROSS CITY	FL	MPAR (2: 120°-300°)
DMN	DEMING (MAGDALEN)	NM	MPAR
FN7	FT GREEN	FL	MPAR
GFA	BOOTLEGGER RIDGE (MALMSTROM)	MT	MPAR
LCH	LAKE CHARLES	LA	MPAR
MLB	MELBOURNE	FL	MPAR
NEN	WHITEHOUSE (JACKSONVILLE)	FL	MPAR (2: 0°-180°)
NEW	SLIDELL (NEW ORLEANS)	LA	MPAR
NQX	KEY WEST	FL	MPAR
NSD	SAN CLEMENTE	CA	MPAR
PAM	TYNDALL AFB	FL	MPAR
PRB	PASO ROBLES	CA	MPAR
QEA	NORTH TRURO	MA	MPAR
QFI	FINLEY	ND	MPAR
QGV	FT FISHER	NC	MPAR
QIE	GIBBSBORO	NJ	None
QJA	EMPIRE	MI	None
QJD	NASHWAUK	MN	MPAR
QKW	MAKAH	WA	MPAR
QLS	LAKESIDE	MT	MPAR
QM8	TAMIAMI	FL	MPAR
QMI	MICA PEAK	WA	MPAR
QMV	MILL VALLEY	CA	MPAR
QNA	MORALES	TX	MPAR
QNW	EAGLE PEAK	TX	MPAR
QOM	KING MOUNTAIN	TX	MPAR
QRJ	JEDBURG	SC	MPAR
QRW	MT LAGUNA	CA	MPAR
QVH	RIVERHEAD (SUFFOLK)	NY	MPAR
QVR	OCEANA	VA	MPAR (2: 30°-210°)
QWA	WATFORD CITY	ND	MPAR
QXU	UTICA (REMSEN)	NY	None

QYA	BUCKS HARBOR	ME	MPAR
QYD	CARIBOU	ME	MPAR
QZA	OILTON	TX	MPAR
QZZ	RAINBOW RIDGE	CA	MPAR
RSG	ROCKSPRINGS	TX	MPAR
SLE	SALEM	OR	MPAR
VBG	VANDENBERG AFB	CA	MPAR

Table A-2 CARSR Sites

Site ID	Site Name	State	Original Type	Radar Replacement
AEX	ALEXANDRIA	LA	FPS-20A	None
AMA	AMARILLO	TX	FPS-67B	None
ATL	MARIETTA	GA	ARSR-1	None
BAM	BATTLE MOUNTAIN	NV	ARSR-2	MPAR
CDC	CEDAR CITY	UT	ARSR-2	MPAR
CLE	BRECKSVILLE (CLEVELAND)	OH	ARSR-1	None
CPV	COOPERSVILLE	MI	FPS-66A	None
DSV	DANSVILLE	NY	ARSR-1	None
FLX	FALLON	NV	FPS-66A	MPAR
FPK	SALT LAKE CITY (FRANCIS PEAK)	UT	ARSR-1	MPAR (2: 350°-170°)
FTW	KELLER	TX	ARSR-1	MPAR
GCK	GARDEN CITY	KS	ARSR-2	None
GJT	GRAND JUNCTION	CO	ARSR-2	MPAR
GUP	GALLUP (FARMINGTON)	NM	ARSR-2	MPAR
HOU	HOUSTON (ELLINGTON AFB)	TX	ARSR-1	None
HTI	HUTCHINSON	KS	FPS-66A	None
IND	INDIANAPOLIS	IN	ARSR-1	None
IRK	KIRKSVILLE	MO	ARSR-3	None
JOL	ELWOOD (JOLIET)	IL	ARSR-3	None
LBF	NORTH PLATTE	NE	ARSR-2	None
LMT	KLAMATH FALLS	OR	FPS-67B	MPAR
LSK	LUSK	WY	ARSR-2	MPAR
MGM	MONTGOMERY	AL	ARSR-1	None
OKC	TINKER AFB	OK	FPS-67B	None
PHX	PHOENIX (HUMBOLDT)	AZ	ARSR-1	None
PIT	OAKDALE	PA	FPS-67B	None
QAS	ANGEL PEAK	NV	FPS-20A	MPAR
QBE	BEDFORD	VA	ARSR-3	None
QBN	BINNS HALL	VA	ARSR-3	MPAR
QBZ	OSKALOOSA	KS	ARSR-2	None
QCF	CLEARFIELD	PA	ARSR-3	None
QCK	CASCADE (BOISE)	ID	ARSR-2	MPAR
QDT	CANTON (DETROIT)	MI	ARSR-1	None
QHA	CUMMINGTON	MA	FPS-67	None
QHB	ST ALBANS	VT	FPS-67B	MPAR
QHN	ASHBURN	GA	ARSR-1	None
QHO	OMAHA	NE	FPS-66A	None
QHZ	HORICON	WI	ARSR-2	None
QJB	GETTYSBURG	SD	FPS-67B	None
QJC	TYLER	MN	ARSR-2	None

QJE	APPLE VALLEY	MN	ARSR-1	None
QJO	ARLINGTON	IA	ARSR-3	None
QLA	SAN PEDRO	CA	ARSR-1	None
QNK	LINCOLNTON	GA	ARSR-3	None
QNM	NEWPORT	MS	ARSR-3	None
QOJ	JOELTON (NASHVILLE)	TN	ARSR-1	None
QPC	HALEYVILLE	AL	FPS-67B	None
QPK	PARKER	CO	ARSR-1	MPAR
QPL	THE PLAINS	VA	ARSR-3	None
QRB	CITRONELLE	AL	ARSR-2	None
QRC	BENTON	PA	FPS-67B	None
QRI	LYNCH	KY	ARSR-2	None
QRL	BENSON	NC	ARSR-1	None
QRM	MAIDEN	NC	ARSR-1	None
QSA	WEST MESA	NM	FPS-66A	None
QSI	LOVELL	WY	ARSR-2	None
QSR	BORON	CA	FPS-67B	MPAR
QTZ	LAGRANGE	IN	ARSR-1	None
QUZ	HANNA CITY	IL	FPS-67B	None
QVA	ASHTON	ID	ARSR-2	MPAR
QVN	FOSSIL	OR	ARSR-3	MPAR
QWC	MESA RICA	NM	ARSR-1	MPAR
QWO	LONDON	OH	ARSR-1	None
QXP	SELIGMAN	AZ	ARSR-3	MPAR
QXR	RUSSELLVILLE	AR	FPS-67A	None
QXS	ODESSA	TX	ARSR-1	MPAR
QYB	BYHALIA (MEMPHIS)	MS	ARSR-1	None
QYS	ROGERS	TX	ARSR-1	MPAR
RBL	RED BLUFF	CA	FPS-67B	None
RKS	ROCK SPRINGS	WY	ARSR-2	MPAR
SEA	SEATTLE (FT LAWTON)	WA	ARSR-1	None
SNI	SAN NICOLAS	CA	ARSR-3	MPAR
STL	ST LOUIS (OVERLAND)	MO	ARSR-1	None
SVC	SILVER CITY	NM	ARSR-2	MPAR
TAD	TRINIDAD	CO	ARSR-2	MPAR
TXK	TEXARKANA	AR	FPS-67	None

Table A-3 NEXRAD Sites

Site ID	Site Name	State	Radar Replacement
KABR	ABERDEEN	SD	MPAR
KABX	ALBUQUERQUE	NM	MPAR
KAKQ	NORFOLK	VA	None
KAMA	AMARILLO	TX	MPAR
KAMX	MIAMI	FL	None
KAPX	NCL MICHIGAN	MI	MPAR
KARX	LA CROSSE	WI	MPAR
KATX	SEATTLE	WA	MPAR
KBBX	BEALE AFB	CA	MPAR
KBGM	BINGHAMTON	NY	MPAR
KBHX	EUREKA (BUNKER HILL)	CA	None
KBIS	BISMARCK	ND	MPAR
KBLX	BILLINGS	MT	MPAR
KBMX	BIRMINGHAM	AL	MPAR
KBOX	BOSTON	MA	None
KBRO	BROWNSVILLE	TX	MPAR
KBUF	BUFFALO	NY	MPAR
KBYX	KEY WEST	FL	None
KCAE	COLUMBIA	SC	MPAR
KCBW	CARIBOU	ME	MPAR (3: 30°-300°)
KCBX	BOISE	ID	MPAR
KCCX	STATE COLLEGE	PA	MPAR
KCLE	CLEVELAND	OH	MPAR
KCLX	CHARLESTON	SC	None
KCRP	CORPUS CHRISTI	TX	MPAR
KCXX	BURLINGTON	VT	None
KCYS	CHEYENNE	WY	MPAR
KDAX	SACRAMENTO	CA	None
KDDC	DODGE CITY	KS	MPAR
KDFX	LAUGHLIN AFB	TX	MPAR (3: 45°-315°)
KDGX	JACKSON/BRANDON	MS	MPAR
KDIX	PHILADELPHIA	NJ	MPAR
KDLH	DULUTH	MN	None
KDMX	DES MOINES	IA	MPAR
KDOX	DOVER AFB	DE	MPAR
KDTX	DETROIT	MI	MPAR

KDVN	QUAD CITIES	IA	MPAR
KDYX	DYESS AFB	TX	MPAR
KEAX	PLEASANT HILL	MO	MPAR
KEMX	TUCSON	AZ	MPAR
KENX	ALBANY	NY	MPAR
KEOX	FT RUCKER	AL	MPAR
KEPZ	EL PASO	NM	None
KESX	LAS VEGAS	NV	MPAR
KEVX	EGLIN AFB	FL	None
KEWX	AUSTIN/SAN ANTONIO	TX	MPAR
KEYX	EDWARDS AFB	CA	None
KFCX	ROANOKE	VA	MPAR
KFDR	ALTUS AFB	OK	MPAR
KFDX	CANNON AFB	NM	None
KFFC	ATLANTA	GA	MPAR
KFSD	SIOUX FALLS	SD	MPAR
KFSX	FLAGSTAFF	AZ	MPAR
KFTG	DENVER	CO	None
KFWS	DALLAS/FT WORTH	TX	None
KGGW	GLASGOW	MT	MPAR
KGJX	GRAND JUNCTION	CO	MPAR
KGLD	GOODLAND	KS	MPAR
KGRB	GREEN BAY	WI	MPAR
KGRK	FT HOOD	TX	None
KGRR	GRAND RAPIDS	MI	MPAR
KGSP	GREER	SC	MPAR
KGWX	COLUMBUS AFB	MS	MPAR
KGYX	PORTLAND	ME	MPAR
KHDX	HOLLOMAN AFB	NM	None
KHGX	HOUSTON	TX	MPAR
KHNX	SAN JOAQUIN VALLEY	CA	MPAR
KHPX	FT CAMPBELL	KY	MPAR
KHTX	NORTHEAST ALABAMA	AL	MPAR
KICT	WICHITA	KS	MPAR
KICX	CEDAR CITY	UT	None
KILN	CINCINNATI	OH	MPAR
KILX	LINCOLN	IL	MPAR
KIND	INDIANAPOLIS	IN	MPAR
KINX	TULSA	OK	MPAR

KIWA	PHOENIX	AZ	MPAR (2: 0°-180°)
KIWX	NORTHERN INDIANA	IN	MPAR
KJAX	JACKSONVILLE	FL	None
KJGX	ROBINS AFB	GA	MPAR
KJKL	JACKSON	KY	MPAR
KLBB	LUBBOCK	TX	MPAR
KLCH	LAKE CHARLES	LA	None
KLGX	LANGLEY HILL	WA	MPAR
KLIX	SLIDELL	LA	None
KLNX	NORTH PLATTE	NE	MPAR
KLOT	CHICAGO	IL	MPAR
KLRX	ELKO	NV	MPAR
KLSX	ST LOUIS	MO	MPAR
KLTX	WILMINGTON	NC	None
KLVX	LOUISVILLE	KY	MPAR
KLWX	STERLING	VA	MPAR
KLZK	LITTLE ROCK	AR	MPAR
KMAF	MIDLAND/ODESSA	TX	None
KMAX	MEDFORD	OR	MPAR (3: 135°-45°)
KMBX	MINOT AFB	ND	MPAR
KMHX	MOREHEAD CITY	NC	MPAR
KMKX	MILWAUKEE	WI	MPAR
KMLB	MELBOURNE	FL	None
KMOB	MOBILE	AL	MPAR
KMPX	MINNEAPOLIS	MN	MPAR
KMQT	MARQUETTE	MI	MPAR
KMRX	KNOXVILLE	TN	MPAR
KMSX	MISSOULA	MT	MPAR
KMTX	SALT LAKE CITY	UT	MPAR
KMUX	SAN FRANCISCO	CA	MPAR
KMVX	FARGO/GRAND FORKS	ND	None
KMXX	MAXWELL AFB	AL	MPAR
KNKX	SAN DIEGO	CA	None
KNQA	MEMPHIS	TN	MPAR
KOAX	OMAHA	NE	MPAR
KOHX	NASHVILLE	TN	MPAR
KOKX	BROOKHAVEN	NY	None
KOTX	SPOKANE	WA	None
KPAH	PADUCAH	KY	MPAR

KPBZ	PITTSBURGH	PA	MPAR
KPDT	PENDLETON	OR	MPAR
KPOE	FT POLK	LA	MPAR (2: 300°-120°)
KPUX	PUEBLO	CO	None
KRAX	RALEIGH/DURHAM	NC	MPAR
KRGX	RENO	NV	MPAR
KRIW	RIVERTON/LANDER	WY	MPAR
KRLX	CHARLESTON	WV	MPAR
KRTX	PORTLAND	OR	MPAR
KSFX	POCATELLO	ID	MPAR
KSGF	SPRINGFIELD	MO	MPAR
KSHV	SHREVEPORT	LA	MPAR
KSJT	SAN ANGELO	TX	MPAR
KSOX	SANTA ANA MTS	CA	None
KSRX	WESTERN ARKANSAS	AR	MPAR
KTBW	TAMPA	FL	None
KTFX	GREAT FALLS	MT	None
KTLH	TALLAHASSEE	MT	None
KTLX	NORMAN	FL	MPAR
KTWX	TOPEKA	KS	MPAR
KTYX	FT DRUM	NY	MPAR
KUDX	RAPID CITY	SD	MPAR
KUEX	GRAND ISLAND	NE	MPAR
KVAX	MOODY AFB	GA	MPAR
KVBX	VANDENBERG AFB	CA	None
KVNX	VANCE AFB	OK	MPAR
KVTX	LOS ANGELES	CA	MPAR
KVWX	EVANSVILLE	IN	MPAR
KYUX	YUMA	AZ	MPAR

GLOSSARY

AGL	Above Ground Level
ARSR	Air Route Surveillance Radar
ASR	Airport Surveillance Radar
ATL	Atlanta
AUC	Area Under the Receiver Operating Curve
AVSET	Automated Volume Scan Evaluation and Termination
CARSR	Common Air Route Surveillance Radar
CHR	Cross-radial Horizontal Resolution
CONUS	Contiguous United States
CPI	Consumer Price Index
CSI	Critical Success Index
CWA	County Warning Area
DHS	Department of Homeland Security
DoD	Department of Defense
DOT	Department of Transportation
DTED	Digital Terrain Elevation Data
EF	Enhanced Fujita
FAA	Federal Aviation Administration
FAR	False Alarm Ratio
FEMA	Federal Emergency Management Administration
FFC	Weather Forecast Office in Peachtree City, Georgia
FVO	Fraction of Vertical Volume Observed
GPN	Ground Position Navigation
ILN	Weather Forecast Office in Wilmington, Ohio
KCMD	Hypothetical Weather Surveillance Radar-1988 Doppler in Cullman, Alabama

KDIX	Weather Surveillance Radar-1988 Doppler in Fort Dix, New Jersey
KFFC	Weather Surveillance Radar-1988 Doppler in Peachtree City, Georgia
KFWS	Weather Surveillance Radar-1988 Doppler in Fort Worth, Texas
KILN	Weather Surveillance Radar-1988 Doppler in Wilmington, Ohio
LRR.	Long-Range Radar
MESO-SAILS	Multiple-Elevation Scan Option for Supplemental Adaptive Intra-volume Low-level Scan
MPAR	Multifunction Phased Array Radar
MUWE	Median Usual Weekly Earnings
NOAA	National Oceanic and Atmospheric Administration
NWRT	National Weather Radar Testbed
NWS	National Weather Service
OKC	Oklahoma City
OUN	Weather Forecast Office in Norman, Oklahoma
PAR	Phased Array Radar
PARISE	Phased Array Radar Innovative Sensing Experiments
POD	Probability of Detection
PPAR	Polarimetric Phased Array Radar
QLCS	Quasi-Linear Convective System
RF	Radio Frequency
SAILS	Supplemental Adaptive Intra-volume Low-level Scan
SENSR	Spectrum Efficient National Surveillance Radar
SPC	Storm Prediction Center
SRTM	Shuttle Radar Tomography Mission
TADW	Terminal Doppler Weather Radar in Andrews Air Force Base, Maryland
TATL	Terminal Doppler Weather Radar in Atlanta, Georgia
TBSS	Three-Body Scatter Signature

TBWI	Terminal Doppler Weather Radar in Baltimore, Maryland
TCLT	Terminal Doppler Weather Radar in Charlotte, North Carolina
TCMH	Terminal Doppler Weather Radar in Columbus, Ohio
TCVG	Terminal Doppler Weather Radar in Covington, Kentucky
TDAY	Terminal Doppler Weather Radar in Dayton, Ohio
TDWR	Terminal Doppler Weather Radar
TEWR	Terminal Doppler Weather Radar in Newark, New Jersey
TMCI	Terminal Doppler Weather Radar in Kansas City, Missouri
TOKC	Terminal Doppler Weather Radar in Oklahoma City, Oklahoma
TOR	Tornado Warning
TPHL	Terminal Doppler Weather Radar in Philadelphia, Pennsylvania
VCP	Volume Coverage Patter
VSL	Value of a Statistical Life
WFO	Weather Forecast Office
WSP	Weather Systems Processor
WSR-88D	Weather Surveillance Radar-1988 Doppler

This page intentionally left blank.

REFERENCES

Ashley, W. S., 2007: Spatial and temporal analysis of tornado fatalities in the United States: 1880–2005. *Wea. Forecasting*, **22**, 1214–1228, https://doi.org/10.1175/2007WAF2007004.1.

Ashley, W. S., and S. M. Strader, 2016: Recipe for disaster: How the dynamic ingredients of risk and exposure are changing the tornado disaster landscape. *Bull. Amer. Meteor. Soc.*, **97**, 767–786, http://dx.doi.org/10.1175/BAMS-D-15-00150.1.

Barnes, L. R., E. C. Gruntfest, M. H. Hayden, D. M. Schultz, and C. Benight, 2007: False alarms and close calls: A conceptual model of warning accuracy. *Wea. Forecasting*, **22**, 1140–1147, https://doi.org/10.1175/WAF1031.1.

Bieringer, P., and P. S. Ray, 1996: A comparison of tornado warning lead times with and without NEXRAD Doppler radar. *Wea. Forecasting*, **11**, 47–52, https://doi.org/10.1175/1520-0434(1996)011<0047:ACOTWL>2.0.CO;2.

Brooks, H. E., and J. Correia, Jr., 2018: Long-term performance metrics for National Weather Service tornado warnings. *Wea. Forecasting*, **33**, 1501–1511, http://dx.doi.org/10.1175/WAF-D-18-0120.1.

Brotzge, J., and W. Donner, 2013: The tornado warning process: A review of current research, challenges, and opportunities. *Bull. Amer. Meteor. Soc.*, **11**, 1715–1733, http://dx.doi.org/10.1175/BAMS-D-12-00147.1.

Brotzge, J., and S. Erickson, 2009: NWS tornado warnings with zero or negative lead times. *Wea. Forecasting*, **24**, 140–154, https://doi.org/10.1175/2008WAF2007076.1.

Brotzge, J., and S. Erickson, 2010: Tornadoes without NWS warning. *Wea. Forecasting*, **25**, 159–172, https://doi.org/10.1175/2009WAF2222270.1.

Brotzge, J., and S. Erickson, and H. Brooks, 2011: A 5-yr climatology of tornado false alarms. *Wea. Forecasting*, **26**, 534–544, https://doi.org/10.1175/WAF-D-10-05004.1.

Brotzge, J., S. E. Nelson, R. L. Thompson, and B. T. Smith, 2013: Tornado probability of detection and lead time as a function of convective mode and environmental parameters. *Wea. Forecasting*, **28**, 1261–1276, https://doi.org/10.1175/WAF-D-12-00119.1.

Brotzge, J., K. Hondl, B. Philips, L. Lemon, E. J. Bass, D. Rude, and D. L. Andra, 2010: Evaluation of distributed collaborative adaptive sensing for detection of low-level circulations and implications for severe weather warning operations. *Wea. Forecasting*, **25**, 173–189, https://doi.org/10.1175/2009WAF2222233.1.

Brown, R. A., and V. T. Wood, 2012: Simulated vortex detection using a four-face phased-array Doppler radar. *Wea. Forecasting*, **27**, 1598–1603, https://doi.org/10.1175/WAF-D-12-00059.1.

Brown, R. A., and V. T. Wood, 2012: The tornadic signature: An update. *Wea. Forecasting*, **27**, 525–530, https://doi.org/10.1175/WAF-D-11-00111.11.

Brown, R. A., V. T. Wood, and D. Sirmans, 2002: Improved tornado detection using simulated and actual WSR-88D data with enhanced resolution. *J. Atmos. Oceanic Technol.*, **19**, 1759–1771, https://doi.org/10.1175/1520-0426(2002)019<1759:ITDUSA>2.0.CO;2.

Burgess, D. W., and L. R. Lemon, 1990: Severe thunderstorm detection by radar. *Radar in Meteorology*, D. Atlas, Ed., Amer. Meteor. Soc., Boston, MA, 619–647.

Cesario, F. J., 1976: Value of time in recreation benefit studies. *Land Econ.*, **52**, 32–41.

Cho, J. Y. N., 2015: Revised Multifunction Phased Array Radar (MPAR) network siting analysis. Project Rep. ATC-425, MIT Lincoln Laboratory, Lexington, MA, 84 pp., https://www.ll.mit.edu/sites/default/files/publication/doc/2018-05/Cho_2015_ATC-425.pdf.

Cho, J. Y. N., and J. M. Kurdzo, 2019a: Weather radar network benefit model for tornadoes. *J. Appl. Meteor. Climatol.*, **58**, 971-987, https://doi.org/10.1175/JAMC-D-18-0205.1.

Cho, J. Y. N., and J. M. Kurdzo, 2019b: Weather radar network benefit model for flash flood casualty reduction. Submitted to *J. Appl. Meteor. Climatol.*

Cho, J. Y. N., and M. E. Weber, 2010: Terminal Doppler Weather Radar enhancements. *Proc. 2010 IEEE Radar Conf.*, Washington, DC, Institute of Electrical and Electronics Engineers, https://doi.org/10.1109/RADAR.2010.5494427.

Cho, J. Y. N., et al., 2015: ASR-9 Weather Systems Processor technology refresh and upgrade. *37th Conf. on Radar Meteorology*, Norman, OK, Amer. Meteor. Soc., 12B.4, https://ams.confex.com/ams/37RADAR/webprogram/Manuscript/Paper275341/RadMet37-Cho-12B4.pdf.

Chrisman, J. N., 2013: Dynamic scanning. *NEXRAD Now*, **22**, NOAA/NWS/Radar Operations Center, Norman, OK, 1–3, https://www.roc.noaa.gov/WSR88D/PublicDocs/NNOW/NNow22c.pdf.

Chrisman, J. N., 2014: The continuing evolution of dynamic scanning. *NEXRAD Now*, **23**, NOAA/NWS/Radar Operations Center, Norman, OK, 8–13, http://www.roc.noaa.gov/WSR88D/PublicDocs/NNOW/NNow23a.pdf.

CIESIN, 2017: Gridded Population of the World, ver. 4 (GPWv4): Population density, rev. 10. NASA Socioeconomic Data and Applications Center, Center for International Earth Science Information Network, Columbia University, Palisades, NY, https://doi.org/10.7927/H4DZ068D.

Crum, T. D., and R. L. Alberty, 1993: The WSR-88D and the WSR-88D operational support facility. *Bull. Amer. Meteor. Soc.*, **74**, 1669–1688, https://doi.org/10.1175/1520-0477(1993)074<1669:TWATWO>2.0.CO;2.

DOT, 2016: Guidance on treatment of the economic value of a statistical life (VSL) in U.S. Department of Transportation Analyses—2016 adjustment. Memorandum to secretarial officers and modal

administrators, Office of the Secretary of Transportation, Department of Transportation, Washington, DC, 13 pp., https://cms.dot.gov/sites/dot.gov/files/docs/2016%20Revised%20Value%20of%20a%20Statistical%20Life%20Guidance.pdf.

Edwards, R., and H. E. Brooks, 2010: Possible impacts of the enhanced Fujita scale on United States tornado data. *25th Conf. on Severe Local Storms*, Denver, CO, Amer. Meteor. Soc., P8.28, http://ams.confex.com/ams/pdfpapers/175398.pdf.

Elsner, J. B., T. Fricker, and W. D. Berry, 2018: A model for U.S. tornado casualties involving interaction between damage path estimates of population density and energy dissipation. *J. Appl. Meteor. Climatol.*, **57**, 2035–2046, https://doi.org/10.1175/JAMC-D-18-0106.1.

FAA, 2018: Spectrum Efficient National Surveillance Radar (SENSR) program announcement. Solicitation 31439, AAQ-300, Federal Aviation Administration, Washington, DC, https://faaco.faa.gov/index.cfm/announcement/view/31439.

Falk, K. W., 1997: Techniques for issuing severe thunderstorm and tornado warnings with the WSR-88D Doppler radar. NOAA Tech. Memo. NWS SR-185, National Weather Service Office, Shreveport, LA, 38 pp., https://repository.library.noaa.gov/view/noaa/6360.

FEMA, 2009: FEMA benefit-cost analysis reengineering (BCAR), version 4.5. Federal Emergency Management Administration, Department of Homeland Security, Washington, DC, 75 pp., https://www.fema.gov/media-library-data/20130726-1738-25045-0690/tornadomethodology.pdf.

Forsyth, D. E., et al., 2005: The National Weather Radar Testbed (phased-array). *32nd Conf. on Radar Meteorology*, Albuquerque, NM, Amer. Meteor. Soc., 24–29, https://ams.confex.com/ams/pdfpapers/21975.pdf.

Fricker, T., J. B. Elsner, and T. H. Jagger, 2017: Population and energy elasticity of tornado casualties. *Geophys. Res. Lett.*, **44**, 3941–3949, http://dx.doi.org/10.1002/2017GL073093.

Gensini, V. A., and H. E. Brooks, 2018: Spatial trends in United States tornado frequency. *Climate Atmos. Sci.*, **1**, 38, https://doi.org/10.1038/s41612-018-0048-2.

Gibbs, J. G., 2016: A skill assessment of techniques for real-time diagnosis and short-term prediction of tornado intensity using the WSR-88D. *J. Oper. Meteor.*, **4**, (13) 170–181, http://dx.doi.org/10.15191/nwajom.2016.0413.

Heinselman, P. L., and S.M. Torres, 2011: High-temporal-resolution capabilities of the National Weather Radar Testbed Phased-Array Radar. *J. Appl. Meteor. Climatol.*, **50**, 579–593, https://doi.org/10.1175/2010JAMC2588.1.

Heinselman, P. L, D. S. LaDue, D. M. Kingfield, and R. Hoffman, 2015: Tornado warning decisions using phased-array radar data. *Wea. Forecasting*, **30**, 57–78, https://doi.org/10.1175/WAF-D-14-00042.1.

Heinselman, P. L, D. L. Priegnitz, K. L. Manross, T. M. Smith, and R. W. Adams, 2008: Rapid sampling of severe storms by the National Weather Radar Testbed Phased Array Radar. *Wea. Forecasting*, **23**, 808–824, https://doi.org/10.1175/2008WAF2007071.1.

Herd, J. S., and M. D. Conway, 2016: The evolution to modern phased array architectures. *Proc. IEEE*, **104**, 519–529, https://doi.org/10.1109/JPROC.2015.2494879.

Istok, M. J., A. Cheek, A. D. Stern, R. E. Saffle, B. R. Klein, N. Shen, and W. M. Blanchard, 2009a: Leveraging multiple FAA radars for NWS operations. *25th Int. Conf. on Interactive Information and Processing Systems for Meteorology, Oceanography, and Hydrology*, Phoenix, AZ, Amer. Meteor. Soc., 10B.2., https://ams.confex.com/ams/pdfpapers/145466.pdf.

Istok, M. J., et al., 2009b: WSR-88D dual polarization initial operational capabilities. *25th Int. Conf. on Interactive Information and Processing Systems (IIPS) for Meteorology, Oceanography, and Hydrology*, Phoenix, AZ, Amer. Meteor. Soc., 15.5, https://ams.confex.com/ams/pdfpapers/148927.pdf.

Kurdzo, J. M., and R. D. Palmer, 2012: Objective optimization of weather radar networks for low-level coverage using a genetic algorithm. *J. Atmos. Oceanic Technol.*, **29**, 807–821, https://doi.org/10.1175/JTECH-D-11-00076.1.

Kurdzo, J. M., and Coauthors, 2017: Observations of severe local storms and tornadoes with the atmospheric imaging radar. *Bull. Amer. Meteor. Soc.*, **98**, 915–935, https://doi.org/10.1175/BAMS-D-15-00266.1.

Kurdzo, J. M., E. F. Joback, J. Y. N. Cho, and P.-E. Kirstetter, 2019: QPE accuracy benefits for weather radar network design. *J. Appl. Meteor. Climatol.*, submitted.

LeClerc, J., and S. Joslyn, 2015: The cry wolf effect and weather-related decision making. *Risk Anal.*, **35**, 385–395, https://doi.org/10.1111/risa.12336.

Lemon, L. R., and C. A. Doswell III, 1979: Severe thunderstorm evolution and mesocyclone structure as related to tornadogenesis. *Mon. Wea. Rev.*, **107**, 1184–1197, https://doi.org/10.1175/1520-0493(1979)107<1184:STEAMS>2.0.CO;2.

Lim, J. R., B. F. Liu, and M. Egnoto, 2019: Cry wolf effect? Evaluating the impact of false alarms on public responses to tornado alerts in the Southeastern United States. *Wea. Climate Soc.*, **11**, 549–563, https://doi.org/10.1175/WCAS-D-18-0080.1.

Manson, S., J. Schroeder, D. Van Riper, and S. Ruggles, 2018: IPUMS National Historical Geographic Information System, version 13.0. University of Minnesota, http://doi.org/10.18128/D050.V13.0.

Michelson, M., W.W. Shrader, and J.G. Wieler, 1990: Terminal Doppler Weather Radar. *Microwave J.*, **33**, 139–148.

NOAA, 2018: Natural hazard statistics. Analyze, Forecast, and Support Office, National Weather Service, National Oceanic and Atmospheric Administration, Silver Spring, MD, http://www.nws.noaa.gov/om/hazstats.shtml.

NRC, 2002: *Weather Radar Technology beyond NEXRAD*. National Research Council, National Academy Press, Washington, DC, 81 pp.

Polger, P. D., B. S. Goldsmith, R. C. Przywarty, and J. R. Bocchieri, 1994: National Weather Service warning performance based on WSR-88D. *Bull. Amer. Meteor. Soc.*, **75**, 203–214, https://doi.org/10.1175/1520-0477(1994)075<0203:NWSWPB>2.0.CO;2.

Press, W. H., S. A. Teukolsky, W. T. Vetterling, and B. P. Flannery, 1992: *Numerical Recipes in C: The Art of Scientific Computing, 2nd Ed*. Cambridge Univ. Press, New York, NY, 994 pp.

Ramsdell, J. V., Jr., and J. P. Rishel, 2007: Tornado climatology of the contiguous United States. Tech. Rep. NUREG/CR-4461, rev. 2, U.S. Nuclear Regulatory Commission, Office of Nuclear Regulatory Research, Washington, DC, 257 pp., https://www.nrc.gov/docs/ML0708/ML070810400.pdf.

R Core Team, 2018: R: A language and environment for statistical computing. R Foundation for Statistical Computing, Vienna, Austria, https://www.R-project.org/.

Schultz, C. J., et al., 2012: Dual-polarization tornadic debris signatures, Part I: Examples and utility in an operational setting. *Electron. J. Oper. Meteor.*, **13**, 120–137.

Simmons, K. M., and D. Sutter, 2005: WSR-88D radar, tornado warnings, and tornado casualties. *Wea. Forecasting*, **20**, 301–310, https://doi.org/10.1175/WAF857.1.

Simmons, K. M., and D. Sutter, 2008: Tornado warnings, lead times, and tornado casualties: An empirical investigation. *Wea. Forecasting*, **23**, 246–258, https://doi.org/10.1175/2007WAF2006027.1.

Simmons, K. M., and D. Sutter, 2009: False alarms, tornado warnings, and tornado casualties. *Wea. Climate Soc.*, **1**, 38–53, https://doi.org/10.1175/2009WCAS1005.1.

Simmons, K. M., and D. Sutter, 2011: *Economic and Societal Impact of Tornadoes*. Amer. Meteor. Soc., Boston, MA, 282 pp.

Smith, B. T., R. L. Thompson, J. S. Grams, C. Broyles, and H. E. Brooks, 2012: Convective modes for significant severe thunderstorms in the contiguous United States. Part I: Storm classification and climatology. *Wea. Forecasting*, **27**, 1114–1135, https://doi.org/10.1175/WAF-D-11-00115.1.

Stailey, J. E., and K. D. Hondl, 2016: Multifunction Phased Array Radar for aircraft and weather surveillance. *Proc. IEEE*, **104**, 649–659, https://doi.org/10.1109/JPROC.2015.2491179.

Stirling, S., 2015: Three out of every four tornado warnings are false alarms. *FiveThirtyEight*, May 27, 2015, Science and Health section, https://fivethirtyeight.com/features/three-out-of-every-four-tornado-warnings-are-false-alarms/.

Strader, S. M., and W. S. Ashley, 2018: Finescale assessment of mobile home tornado vulnerability in the central and southeast United States. *Wea. Climate Soc.*, **10**, 797–812, https://doi.org/10.1175/WCAS-D-18-0060.1.

Sutter, D., and S. Erickson, 2010: The time cost of tornado warnings and the savings with storm-based warnings. *Wea. Climate Soc.*, **2**, 103–112, https://doi.org/10.1175/2009WCAS1011.1.

Torres, S., and C. Curtis, 2006: Design considerations for improved tornado detection using superresolution data on the NEXRAD network. Preprints, *3rd European Conf. on Radar Meteorology and Hydrology (ERAD)*, Barcelona, Spain, https://ams.confex.com/ams/pdfpapers/116240.pdf.

USCB, 2016: B25033: Total population in occupied housing units by tenure by units in structure. 2011–2015 American Community Survey 5-Year Estimates, U. S. Census Bureau, Washington, DC, http://factfinder2.census.gov.

Weber, M. E., J. Y. N. Cho, J. S. Herd, J. M. Flavin, W. E. Benner, and G. S. Torok, 2007: The next-generation multimission US surveillance radar network. *Bull. Amer. Meteor. Soc.*, **88**, 1739–1751, https://doi.org/10.1175/BAMS-88-11-1739.

Weber, M. E., J. Y. N. Cho, and H. G. Thomas, 2017: Command and control for multifunction phased array radar. *IEEE Trans. Geosci. Remote Sens.*, **55**, 5899–5912, https://doi.org/10.1109/TGRS.2017.2716935.

Weber, M. E., K. D. Hondl, M. J. Istok, and R. E. Saffle, 2018: NOAA's Spectrum Efficient National Surveillance Radar (SENSR) research program. *34th Conf. on Environmental Information Processing Technologies*, Austin, TX, Amer. Meteor. Soc., 10.1, https://ams.confex.com/ams/98Annual/webprogram/Paper337206.html.

Wilson, K. A., P. L. Heinselman, C. M. Custer, D. M. Kingfield, and Z. Kang, 2017: Forecaster performance and workload: Does radar update time matter? *Wea. Forecasting*, **32**, 253–274, https://doi.org/10.1175/WAF-D-16-0157.1.

Wood, V. T. and R. A. Brown, 1997: Effects of radar sampling on single-Doppler velocity signatures of mesocyclones and tornadoes. *Wea. Forecasting*, **12**, 928–938, https://doi.org/10.1175/1520-0434(1997)012<0928:EORSOS>2.0.CO;2.

Zhang, G., R. Doviak, D. Zrnic, and J. Crain, 2008: Phased array radar polarimetry for weather sensing: Challenges and opportunities. *2008 IEEE Geoscience and Remote Sensing Symp. (IGARSS)*, **5**, Boston, MA, IEEE, 449–452, https://doi.org/10.1109/IGARSS.2008.4780125.

Zrnic, D. S. and R. J. Doviak, 1976: Effective antenna pattern of scanning radars. *IEEE Trans. Aerosp. Electron. Syst.*, **12**, 551–555, https://doi.org/10.1109/TAES.1976.308254.

Zrnic, D. S., J. F. Kimpel, D. E. Forsyth, A. Shapiro, G. Crain, R. Ferek, J. Heimmer, W. Benner, F. T. J. McNellis, and R. J. Vogt, 2007: Agile-beam phased array radar for weather observations. *Bull. Amer. Meteor. Soc.*, **88**, 1753–1766, https://doi.org/10.1175/BAMS-88-11-1753.

REPORT DOCUMENTATION PAGE

Form Approved
OMB No. 0704-0188

1. REPORT DATE *(DD-MM-YYYY)*	**2. REPORT TYPE**	**3. DATES COVERED** *(From - To)*
29-08-2019	Project Report	

4. TITLE AND SUBTITLE

Monetized Weather Radar Network Benefits for Tornado Cost Reduction

5a. CONTRACT NUMBER
FA8702-15-D-0001

5b. GRANT NUMBER

5c. PROGRAM ELEMENT NUMBER

6. AUTHOR(S)

J. Cho, J. Kurdzo

5d. PROJECT NUMBER
10215

5e. TASK NUMBER
452

5f. WORK UNIT NUMBER

7. PERFORMING ORGANIZATION NAME(S) AND ADDRESS(ES)

MIT Lincoln Laboratory
244 Wood Street
Lexington, MA 02421-6426

8. PERFORMING ORGANIZATION REPORT NUMBER

NOAA-35

9. SPONSORING / MONITORING AGENCY NAME(S) AND ADDRESS(ES)
Kurt Hondl
NOAA National Severe Storms Laboratory
120 David L Boren Blvd.
Norman, OK 73032

10. SPONSOR/MONITOR'S ACRONYM(S)
NOAA

11. SPONSOR/MONITOR'S REPORT NUMBER(S)

12. DISTRIBUTION / AVAILABILITY STATEMENT

Approved for public release: distribution unlimited.

13. SUPPLEMENTARY NOTES

14. ABSTRACT

A monetized tornado benefit model is developed for arbitrary weather radar network configurations. Geospatial regression analyses indicate that improvement in two key radar coverage parameters—fraction of vertical space observed and cross-range horizontal resolution—lead to better tornado warning performance as characterized by tornado detection probability and false alarm ratio. Previous experimental results showing faster volume scan rates yielding greater warning performance, including increased lead times, are also incorporated into the model. Enhanced tornado warning performance, in turn, reduces casualty rates. In combination, then, it is clearly established that better and faster radar observations reduce tornado casualty rates. Furthermore, lower false alarm ratios save cost by cutting down on people's time lost while taking shelter.

15. SUBJECT TERMS

16. SECURITY CLASSIFICATION OF:			**17. LIMITATION OF ABSTRACT**	**18. NUMBER OF PAGES**	**19a. NAME OF RESPONSIBLE PERSON**
a. REPORT	**b. ABSTRACT**	**c. THIS PAGE**			**19b. TELEPHONE NUMBER** *(include area code)*
Unclassified	Unclassified	Unclassified	Same as report	88	

This page intentionally left blank.